North Indian Ocean Circulation Since the Last Deglaciation as Inferred From New Elemental Ratio Records for Benthic Foraminifera Hoeglundina elegans

Ruifang Ma, Sophie Sepulcre, Franck Bassinot, Frédéric Haurine, Nadine Tisnérat-laborde, Christophe Colin

Paleoceanography and Paleoclimatology

RESEARCH ARTICLE
10.1029/2019PA003801

North Indian Ocean Circulation Since the Last Deglaciation as Inferred From New Elemental Ratio Records for Benthic Foraminifera *Hoeglundina elegans*

Ruifang Ma[1], Sophie Sépulcre[1], Franck Bassinot[2], Frédéric Haurine[1], Nadine Tisnérat-Laborde[2], and Christophe Colin[1]

[1]GEOPS, Université Paris-Sud, CNRS, Université Paris-Saclay, Rue du Belvédère, Orsay, France, [2]LSCE/IPSL, CEA CNRS UVSQ, Gif-sur-Yvette, France

Key Points:
- We produced high-resolution records of benthic foraminiferal elemental ratios, $\delta^{18}O$, and $\delta^{13}C$ from two cores from the northern Indian Ocean
- Evaluation of past IWT from the Mg/Li ratio and the $\delta^{18}O$ since last deglaciation exhibit millennial-scale changes
- Variations of the IW $\Delta[CO_3^{2-}]$ calculated from *H. elegans* Sr/Ca are related to atmospheric CO_2 changes on glacial-interglacial timescales

Supporting Information:
- Supporting Information S1
- Data Set S1
- Data Set S2

Correspondence to:
R. Ma,
maruifang89@hotmail.com

Citation:
Ma, R., Sépulcre, S., Bassinot, F., Haurine, F., Tisnérat-Laborde, N., & Colin, C. (2020). North Indian Ocean circulation since the last deglaciation as inferred from new elemental ratio records for benthic foraminifera *Hoeglundina elegans*. *Paleoceanography and Paleoclimatology*, *35*, e2019PA003801. https://doi.org/10.1029/2019PA003801

Received 4 NOV 2019
Accepted 24 APR 2020
Accepted article online 18 MAY 2020

Abstract The evolution of intermediate circulation in the northern Indian Ocean since the last deglaciation has been reconstructed from two marine cores located at intermediate depths off the southern tip of India (MD77-191) and in the northern Bay of Bengal (BoB) (MD77-176). Benthic foraminiferal $\delta^{13}C$, seawater carbonate ion concentration ($[CO_3^{2-}]$) estimated from the Sr/Ca, and paleotemperature reconstructed on the basis of the Mg/Li of aragonite benthic species *Hoeglundina elegans* were used to trace the evolution of past intermediate-deepwater masses and to constrain ocean-atmosphere exchanges during the two-stage increase in atmospheric CO_2 across the last deglaciation. The intermediate water $[CO_3^{2-}]$ was mainly affected by changes in the ocean alkalinity inventory, associated with the modulation of atmospheric CO_2 on glacial-interglacial timescales. Higher benthic foraminiferal $\delta^{13}C$, depleted $[CO_3^{2-}]$, and decreased benthic-planktonic ^{14}C age offsets at intermediate water depths suggest a release of deep-sea CO_2 to the atmosphere through the Antarctic Intermediate Water (AAIW) in the Southern Ocean during the 17–15.2 and 12.6–10.5 cal kyr BP time intervals. In addition, the decreased *H. elegans* Mg/Li record seems to reflect an increased contribution of cold water mass during the 17–15.2 and 12.6–11.9 cal kyr BP intervals and throughout the Holocene. In contrast, two warm events occurred in the 15–13.3 and 11–10.3 cal kyr BP time intervals. During the late Holocene, a decrease in the intermediate water $[CO_3^{2-}]$ indicates a contribution to atmospheric CO_2 rise since 8 cal kyr BP, due to the depleted global ocean alkalinity and/or the variations in surface productivity (at least for MD77-191).

1. Introduction

Atmospheric CO_2 records from ice cores in Antarctica exhibit variations at glacial-interglacial and millennial timescales over the last 800 kyr that are correlated to global climate changes (Lisiecki & Raymo, 2005; Lüthi et al., 2008). This indicates that the climate system and, in particular, the Earth's heat budget and temperature are highly sensitive to variations in CO_2 greenhouse gas (IPCC, 2013). Past variations in the global carbon cycle are, therefore, a key element to understand the processes controlling atmospheric CO_2 and its relationships to climate changes. As the ocean is the largest external carbon reservoir that can exchange rapidly with the atmosphere, changes in the oceanic carbon pool are strongly linked to past atmospheric CO_2 variations (Broecker & Peng, 1982), through complex feedback relationships. A decrease in atmospheric CO_2 can drive Earth cooling, and such cooling can, in turn, result in a further decrease in atmospheric CO_2 by enhancing carbon solubility and thus carbon storage in ocean waters. For instance, such a change led to a net decrease of ~15 ppm in atmospheric CO_2 during the glacial period (Brovkin et al., 2007; Sigman & Boyle, 2000; Yu, Anderson, & Rohling, 2014). At a shorter timescale, abrupt millennial events, such as during the last deglaciation, require more complex ocean processes, involving changes in ocean biogeochemistry and circulation.

Exchanges of carbon through the ocean and to/from the atmosphere occur through changes in the dissolved inorganic carbon (DIC) system (e.g., Anderson et al., 2009; Ridgwell & Zeebe, 2005; Sigman & Boyle, 2000). Among the DIC species, the carbonate ion concentration ($[CO_3^{2-}]$) is a particularly important one as it determines the seawater carbonate saturation state with respect to the calcium carbonates in the water column as well as at the seafloor. Variations in seawater $[CO_3^{2-}]$, by driving changes in the

preservation/dissolution of sedimentary carbonates, make this fraction an active player of the ocean and global carbon cycle. Thus, reconstructing past seawater [CO_3^{2-}] variations is mandatory to better constrain the processes and mechanisms controlling past global carbon cycle.

As a means of reconstructing bottom water parameters over a geological timescale, benthic foraminifera elemental/Ca ratios have received increasing attention over recent decades (e.g., Boyle et al., 1995; Boyle & Keigwin, 1985; Marchitto et al., 2018; Raitzsch et al., 2011; Yu et al., 2008). For instance, the Mg/Ca in benthic foraminifera has been widely used to reconstruct bottom water temperature changes (e.g., Barrientos et al., 2018; Lear et al., 2002; Marchitto et al., 2007; Martin et al., 2002; Rosenthal et al., 1997; Yu & Broecker, 2010). However, this proxy is also sensitive to bottom water carbonate ion saturation ($\Delta[CO_3^{2-}]$, defined as the difference between [CO_3^{2-}] and [$CO_3^{2-}]_{sat}$) (e.g., Bryan & Marchitto, 2008; Marchitto et al., 2018; Rosenthal et al., 2006; Yu & Elderfield, 2008). Other elemental/Ca ratios, such as the benthic foraminifera Li/Ca and Sr/Ca, have been shown to covary with both past bottom temperatures and $\Delta[CO_3^{2-}]$ (e.g., Bryan & Marchitto, 2008; Doss et al., 2018; Hall & Chan, 2004; Marchitto et al., 2018; Rosenthal et al., 2006). More recent studies have demonstrated that the benthic foraminiferal U/Ca, Li/Ca, and Sr/Ca are also promising proxies for the marine dissolved carbon/carbonate system (Bryan & Marchitto, 2008; Keul et al., 2013; Raitzsch et al., 2011; Yu, Elderfield, Jin, Tomascak, & Rohling, 2014); they can thus increase our ability to fully reconstruct past changes in the intermediate and deepwater chemistry linked to the global carbon cycle (Came et al., 2008; Makou et al., 2010; Poggemann et al., 2017; Yu et al., 2008).

Most of the studies referred to above were devoted to calcitic foraminifera. Only a few studies have focused on benthic foraminifera *Hoeglundina elegans*, since this aragonite species is not widely found in the sediment due to its higher sensitivity to dissolution than calcitic foraminifera (Marchitto et al., 2018; Rosenthal et al., 2006). Previous works suggest that Mg/Ca, Li/Ca, and Sr/Ca in *H. elegans* could also be used as paleoproxies for both carbonate ion concentration and temperature (e.g., Bryan & Marchitto, 2008; Hall & Chan, 2004; Marchitto et al., 2018; Rosenthal et al., 2006).

Furthermore, most of these studies that apply elemental ratios have focused on the Atlantic Ocean (e.g., Makou et al., 2010; Poggemann et al., 2017; Yu et al., 2008). As the northern Indian Ocean plays an important role in global ocean circulation in terms of deepwater ventilation and stratification (e.g., Ahmad et al., 2008, 2012; Bryan et al., 2010; Raza et al., 2014), it has received increasing attention over recent decades (e.g., Bryan et al., 2010; Ma et al., 2019; Sijinkumar et al., 2016; Yu et al., 2018). However, no continuous, high-resolution benthic foraminiferal elemental ratio records have been produced for this area.

In this study, we investigated benthic and planktonic foraminiferal $\delta^{13}C$, $\delta^{18}O$, and elemental ratios from two cores located at intermediate water depths off the southern tip of India and in the northeastern Bay of Bengal (BoB); our aim is to better constrain the temporal evolution of the source and ventilation of intermediate water mass in the northern Indian Ocean. We explored the potential of the Mg/Li and Sr/Ca ratios of *H. elegans* as proxies to reconstruct past changes in the temperature and [CO_3^{2-}], respectively. Reconstructing past variations in [CO_3^{2-}] and comparing our results with other areas as well as with atmospheric CO_2 records allow us to better understand the relationships between past changes in intermediate ocean circulation and variations in the global carbon cycle.

2. Material and Hydrological Settings

Cores MD77-191 and MD77-176 were collected off the southern tip of India on the edge of the Arabian Sea (07°30′N–76°43′E, 1,254 m water depth) and in the northeastern BoB (14°30′5 N–93°07′6E, 1,375 m water depth), respectively, during the OSIRIS III cruise of the N.0 *Marion Dufresne* in 1977 (Figure 1). These two cores cover a similar range of [CO_3^{2-}] (75 μmol/kg for MD77-191 and 82 μmol/kg for MD77-176) in the modern ocean (supporting information Figure S1). The modern [CO_3^{2-}] values are calculated using CO_2sys.xls (Ver. 12) based on the data collection from the Global Alkanity & TCO_2 data sets (Goyet et al., 2000; Pelletier et al., 2005).

Today, the surface water masses above 150 m in the Arabian Sea correspond to the Arabian Sea High Salinity Water (ASHS; salinity 36.5 psu) (Talley et al., 2011). In contrast, in the BoB, the surface water shallower than 100 m, that is, Bay of Bengal Surface Water (BoBSW), is much fresher (salinity ~31 psu) because of the

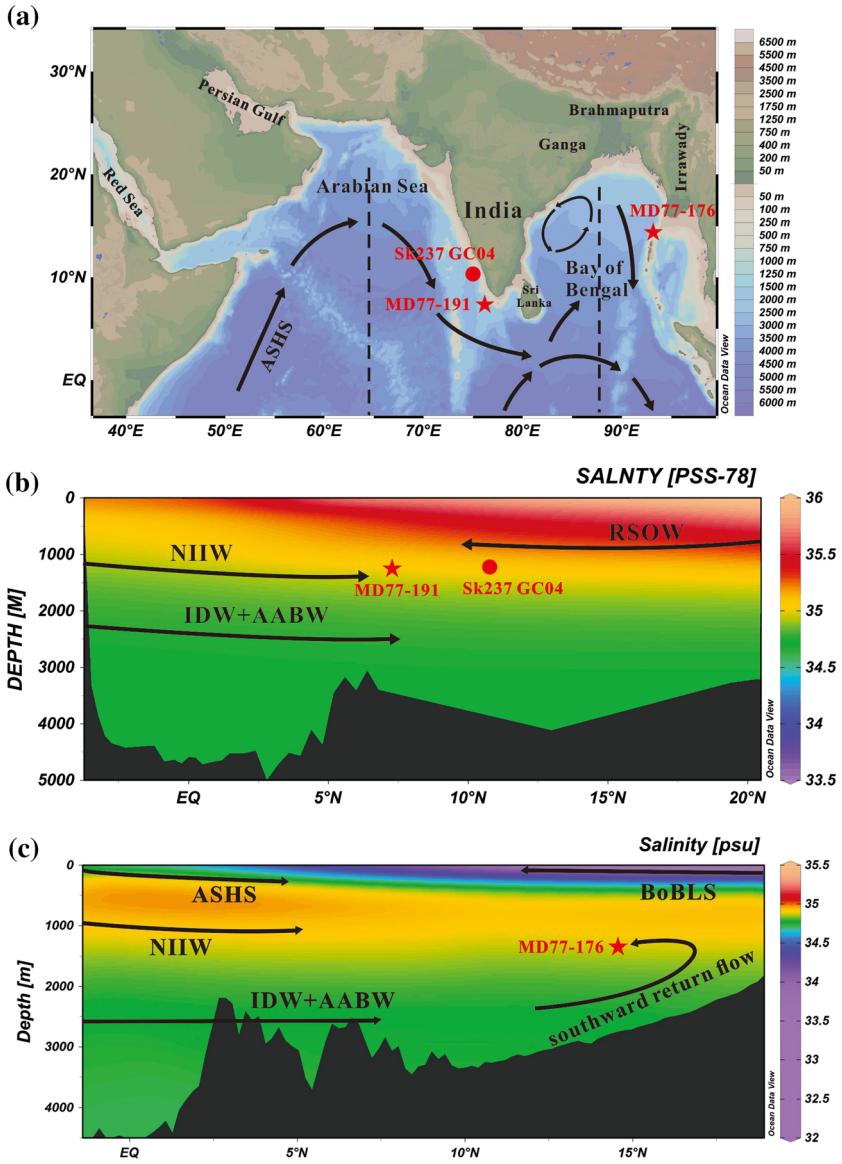

Figure 1. (a) Geographical setting, locations of MD77-191 (red star) in the Arabian Sea, MD77-176 (red star) in the Bay of Bengal, and Reference Site SK237 GC04 (red circle, Naik et al., 2017). The black arrows indicate the general direction of surface circulation in the northern Indian Ocean drifted by Southwest Monsoon (Schott & McCreary, 2001). (b and c) Salinity (psu, colored shading) depth-latitude section using Ocean Data View (ODV) software (Schlitzer, 2015) and vertical distribution of water masses in the Arabian Sea and Bay of Bengal (N-S cross section). AABW = Antarctic Bottom Water; ASHS = Arabian Sea High Salinity Water; BoBLS = Bay of Bengal Low Salinity Water; IDW = Indian Deep Water; NIIW = North Indian Intermediate Water; RSOW = Red Sea Overflow Water.

considerable input from rivers (Talley et al., 2011). The surface mixed layer and the boundary currents in the Arabian Sea and in the BoB are directly controlled by wind forcing and, therefore, display changes related to the seasonal reversal of the Indian monsoon wind system (Figure 1). The surface waters at the site of MD77-191 and MD77-176 are a mix of high-salinity ASHS and low-salinity BoBSW, respectively (Talley et al., 2011; Tomczak & Godfrey, 2003). MD77-191 is also located in the summer upwelling area of the Arabian Sea, and the average depth of the permanent thermocline is around 100 m (Ravichandran et al., 2012).

The main intermediate water masses in the Indian Ocean are Antarctic Intermediate Water (AAIW), Red Sea Overflow Water (RSOW), and Indonesian Intermediate Water (IIW) (Talley et al., 2011; You, 1998). The northward extension of AAIW in the Indian Ocean reaches only as far as 10°S in the modern Indian

Ocean (Lynch-Stieglitz et al., 1994). Red Sea Water is a high-salinity intermediate water, and it fills the Arabian Sea (between 400 and 1,400 m) (Beal et al., 2000; Talley et al., 2011). RSOW spreads eastward to the eastern boundary at 5°N and flows through the much stronger western boundary toward the Agulhas (Beal et al., 2000; Talley et al., 2011; You, 1998). Thus, RSOW could impact upon the MD77-191 core site at the southern tip of India but should make only a small contribution at Core Site MD77-176 in the BoB. IIW originates from the Pacific Central Water and enters the BoB via the Indonesian through flow. IIW flows clockwise at thermocline levels in the BoB (You, 1998).

The deepwater masses of the northern Indian Ocean are characterized by a mixture of Atlantic and Antarctic water masses (Reid, 2003; Talley et al., 2011). Between 1,200 and 3,800 m, the dominant deep water is Indian Deep Water (IDW), originating from the Circumpolar Deep Water and NADW (Tomczak & Godfrey, 2003; You & Tomczak, 1993). Below 3,800 m, the abyssal basins are bathed chiefly by the Antarctic Bottom Water (AABW) (Reid, 2003; Tomczak & Godfrey, 2003). However, AABW only reaches the southern part of the BoB as most of the bay is shallower than 4,000 m (Tomczak & Godfrey, 2003). In the BoB, the bottom water upwells when it moves northward (Talley et al., 2011); thus, changes in bottom waters are transferred upward to shallower water masses.

3. Methods

3.1. $\delta^{18}O$ and $\delta^{13}C$ Analyses From Core MD77-191

Stable oxygen ($\delta^{18}O$) and carbon ($\delta^{13}C$) isotope records for MD77-176 have already been published in Ma et al. (2019). For Core MD77-191, measurements were performed on well-preserved (clean and intact) samples of the planktonic foraminifera *Globigerinoides ruber* (250–315 μm fraction) and the endobenthic foraminifera *Uvigerina peregrina* (250–315 μm fraction). As *U. peregrina* is an infaunal benthic foraminiferal species, the $\delta^{13}C$ values may reflect pore water isotopic compositions rather than deepwater signature. To obtain a high-resolution benthic $\delta^{13}C$ record that would more accurately reflect bottom water changes, epibenthic foraminifera *Cibicidoides wuellerstorfi* and *Cibicidoides pachyderma* were also analyzed.

These stable isotope analyses were performed on approximately 4 to 8 clean and well-preserved specimens per sample using a Finnigan MAT 251 mass spectrometer at the Laboratoire des Sciences du Climat et de l'Environnement (LSCE, France). The $\delta^{18}O$ and $\delta^{13}C$ values are presented relative to the Pee Dee Belemnite (PDB) scale through calibrations performed with standards from the National Bureau of Standards (NBS). The mean external reproducibility of carbonate standards is ±0.05‰ for $\delta^{18}O$ and ±0.03‰ for $\delta^{13}C$.

3.2. Analytical Protocols for Elemental Ratios

Mg/Ca, Sr/Ca, U/Ca, and Li/Ca ratios were measured in shells of the epifaunal benthic foraminifera *H. elegans* from MD77-191. Only the Mg/Ca and Sr/Ca results are available for MD77-176 due to the paucity of material and the difficulty in measuring the Li/Ca and U/Ca ratios on very small samples. *H. elegans* is an epifaunal species that grows on the sediment-seawater interface, thus minimizing the influence of pore water composition on the elemental ratios (Lutze & Thiel, 1989). Each sample contained approximately 8–15 individual foraminifera larger than 250 μm. The foraminiferal test samples were crushed open between two glass plates. The resulting fragments were ultrasonically cleaned to remove clays and then subjected to oxidative and reductive protocols to remove organic matter and oxides following methods described by Boyle and Keigwin (1985) and Barker et al. (2003). Samples were dissolved in 0.075 N HNO_3 and analyzed using a single collector sector field high-resolution inductively coupled plasma mass spectrometer (HR-ICP-MS) Thermo Element XR hosted at the Laboratory GEOPS (University Paris-Sud, France).

Instrumental settings used for trace element analyses are listed in Data Set S1. The instrument sensitivity was optimized daily using 100 ppt tuning standard solutions. Given the limited amount of solution obtained after dissolution of the foraminifera samples, a high efficiency PFA MicroFlow Nebulizer (ES-2000-3503-080) was used and resulted in an uptake rate of 50 μl/min. Aliquots of samples were first analyzed for Ca concentrations, and after, the remaining solutions were diluted to reach a Ca concentration of ~50 ppm for the second analyses of Mg, Sr, Cd, Li, B, Ba, and U (Yu et al., 2005). One measurement requires 1 ml solution.

Table 1
Calibrated AMS ^{14}C Age Determined on Planktonic (10 Data Taken From Bassinot et al., 2011)

Depth (cm)	Calendar age (yr BP)	Taxa	^{14}C age (yr)	1 sigma error (±yr)
28	1,526	*G. bulloides*	1,970	60
76	2,226	*G. bulloides*	2,560	70
127	2,797	*G. bulloides*	3,020	60
175	3,567	*G. bulloides*	3,660	60
222	4,236	*G. bulloides*	4,160	60
271	5,070	*G. bulloides*	4,790	60
373	6,582	*G. bulloides*	6,150	80
425	8,757	*G. bulloides*	8,230	90
482	9,648	*G. bulloides*	8,970	80
550	11,294	*G. ruber*	10,300	50
580	13,285	*G. ruber*	11,810	50
594	14,258	*Pteropods* sp.	12,630	190
710	16,142	*G. ruber*	13,820	60

Note. ^{14}C ages were converted into calendar years (cal. yr BP, BP = AD 1950) USING THE CALIB REV. 7.1 SOFTWARE (STUIVER & BRAZIUNAS, 1993).

The procedures here are similar to the method described by Yu et al. (2005). Two series of mother standard solutions were prepared for elemental ratio analyses. The first six standard solutions were Mn, Al, and Fe mixtures with linear Ca concentration (0.5–7 ppm) to get more precise Ca concentration dilutions for the second run. Then, seven multi-element standard stock solutions (J0–J6) were prepared gravimetrically by spiking a 1,000 μg/ml Ca standard with appropriate amounts of Mg, Sr, Cd, Li, B, Ba, and U monoelemental 1,000 μg/ml certified ICP-MS-grade stock solutions. The ratios of stock solutions were spaced linearly to contain the natural ratio ranges expected in both planktonic and benthic foraminifera. Working mother standards were made by diluting the stock standard solutions with 0.1 N HNO_3 to get calcium concentrations of 50 ppm.

Sample solutions were systematically adjusted at 50 ppm Ca through dilution using 0.1 N HNO_3. A blank consisting of the same 0.1 N HNO_3 used to dilute the standards and samples was also analyzed. The elemental blanks are better than 0.14% for Mg, 0.02% for Sr, 5.3% for Li, and 0.05% for U. All raw intensities (including standards) were corrected by removing the specific blank intensity values. Drift corrections were performed during daily analyses by bracketing and linear regression estimated using standards interspersed every four samples. Standard curves were used to calculate elemental/Ca ratios, and coefficients of determination (r^2) were always >0.9999 for all elemental ratios. The mean reproducibility is 2% for Mg/Ca, 0.9% for Sr/Ca, 0.2% for Li/Ca, and 3.5% for U/Ca.

4. Chronological Framework of the Studied Cores

The age model of Core MD77-191 was established using nine accelerator mass spectrometry (AMS) ^{14}C dates from monospecific planktonic foraminifer *Globigerina bulloides* (Bassinot et al., 2011), one ^{14}C date from pteropods (Mléneck, 1997), and three ^{14}C dates obtained from planktonic foraminifera *G. ruber* measured with the *ECHo*MICADAS at the LSCE, France (see the analytical method in detail in Ma et al., 2019) (Table 1). The ^{14}C dates were converted to calendar dates using CALIB Rev. 7.1 software (Stuiver & Braziunas, 1993) and the marine calibration data set (Reimer et al., 2013) and corrected for a surface marine reservoir of around 400 yr. MD77-191 provides a continuous record spanning the last 17 kyr BP with an average sedimentation rate of about 53 and up to 90 cm/kyr for the Holocene.

The age model of Core MD77-176 was previously established using 31 planktonic foraminifera (*G. ruber*) AMS ^{14}C dates combined with the MD77-176 oxygen isotope record obtained on planktonic foraminifera *G. ruber*, which was correlated to the GISP2 Greenland ice core record (Marzin et al., 2013). MD77-176 displays high accumulation rates (average ~25 and up to 40 cm/kyr for the Holocene) and provides a high-resolution record for the period since 40 cal kyr BP.

5. Results

Results obtained from Cores MD77-191 and MD77-176 reveal millennial-scale events that punctuated the last deglaciation. However, we will not discuss the significance of these variations at the core sites in terms of Heinrich Stadial 1, Younger Dryas or Bølling-Allerød events, because the timing of these events, especially from where they have been described in the northern Atlantic Ocean, may be not strictly synchronous with observations from the northern Indian Ocean, as already observed in previous works from the area (e.g., Ma et al., 2019). Thus, we prefer to use the labeling of the time intervals rather than interpreting them in terms of deglacial climate events.

5.1. Stable Isotope Results From Core MD77-191

Stable isotope analyses were performed on planktonic foraminifera *G. ruber* and on benthic foraminifera *C. pachyderma*, *C. wuellerstorfi*, and *U. peregrina* from MD77-191 to produce the most complete records. Benthic $\delta^{18}O$ values were obtained from *U. peregrina*, which is known to record the calcite $\delta^{18}O$ at

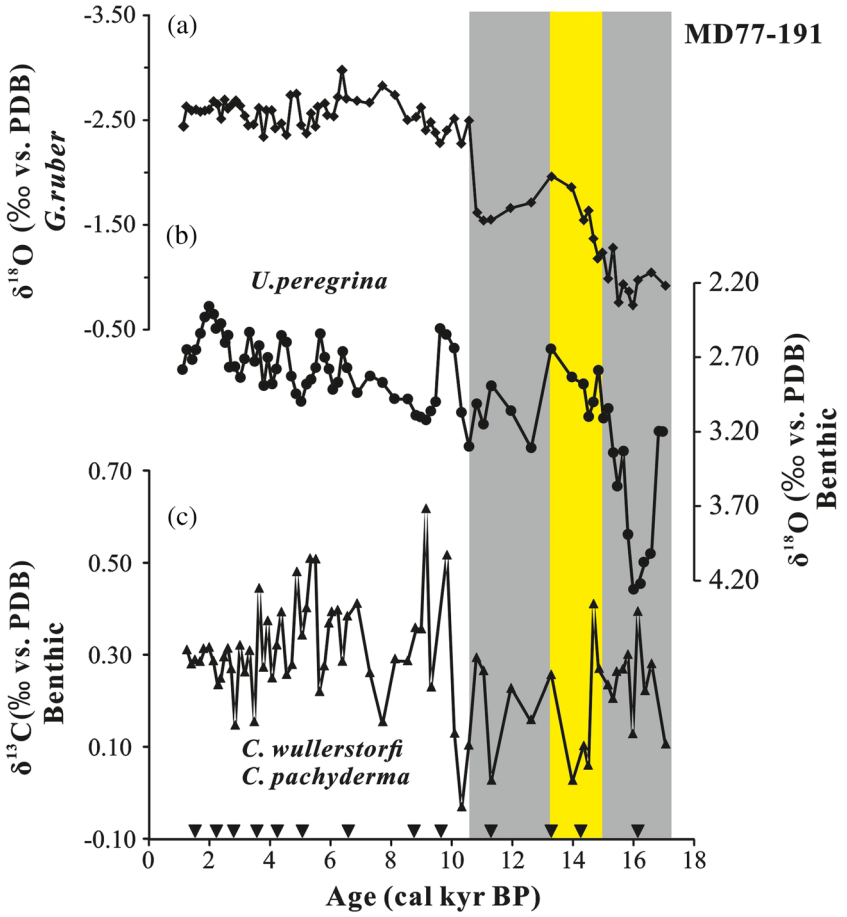

Figure 2. (a) $\delta^{18}O$ records of the planktonic foraminifera *G. ruber*, (b) benthic $\delta^{18}O$, and (c) $\delta^{13}C$ records for MD77-191. The black inverted triangles represent the ^{14}C calculated calendar age points (Bassinot et al., 2011). The gray-shaded intervals mark the two-step increase in atmospheric CO_2 (Monnin et al., 2001), and the yellow-shaded interval marks the 15–13.3 cal kyr BP interval.

equilibrium (e.g., Shackleton, 1974). The $\delta^{13}C$ obtained from *C. wuellerstorfi* is known in the literature to record the bottom water $\delta^{13}C$ at equilibrium (Duplessy et al., 1984; Zahn et al., 1986), without any microhabitat effect (except in some special areas, like Southern Ocean, Mackensen et al., 1993). Because of the lack of *C. wuellerstorfi*, and in order to get a higher resolution, we completed the $\delta^{13}C$ record with results from *C. pachyderma*. We corrected the values from *C. pachyderma* to *C. wuellerstorfi* by using the average difference of 0.27‰ we measured between both species, obtained from 19 pair measurements of samples where the two species coexisted (Data Set S2 and Figure S2).

The $\delta^{18}O$ of *G. ruber* was enriched during the last deglaciation compared with the Holocene (Figure 2). A marked maximum in *G. ruber* $\delta^{18}O$ is evident during the early deglaciation, reaching −0.7‰ at 16 cal kyr BP. After that, the $\delta^{18}O$ displays a general decrease and reaches a more depleted level during the Holocene with an average of ~ −2.58‰. In addition, the general trend is punctuated by higher values of ~ −1.53‰ in the interval between 12.6 and 10.5 cal kyr BP (the late deglaciation).

Down-core benthic $\delta^{18}O$ values range between 2.36‰ and 4.25‰ (Figure 2). The most enriched $\delta^{18}O$ value (4.25‰) was found during the last deglaciation period (16 cal kyr BP), whereas the most depleted (2.36‰) occurred in the late Holocene (2.36 cal kyr BP). In the late part of the deglaciation, the $\delta^{18}O$ shows a shift toward higher values of around ~3‰ in the 12.6–10.5 cal kyr BP. This interval is followed by a decrease of $\delta^{18}O$ from 10 cal kyr BP to the core top (mean value of 2.75‰).

The *Cibicidoides* $\delta^{13}C$ values of MD77-191 range from −0.04‰ to 0.62‰ (Figure 2). Although the record seems quite noisy, an increase (~0.11‰) in the $\delta^{13}C$ from the last deglaciation to the Holocene could be

observed. In addition, shorter-scale events occurred during the last deglaciation; the *Cibicidoides* $\delta^{13}C$ values increased during the time intervals 17–15.2 and 12.6–10.5 cal kyr BP and decreased (~0.03‰) at around 15–13.3 cal kyr BP. From 10.3 to about 9 cal kyr BP, the *Cibicidoides* $\delta^{13}C$ record suggests that considerable oscillations occurred with high peak values (0.52–0.62‰) at around 9.8–9.1 cal kyr BP. Then, the $\delta^{13}C$ records display a decrease during the middle and late Holocene, with a mean value of ~0.31‰ for *Cibicidoides* $\delta^{13}C$.

5.2. Elemental Ratios in *H. elegans* From Cores MD77-191 and MD77-176

To check the robustness of our results and the potential diagenetic imprint (i.e., oxides), the Mn/Ca ratio was systematically measured. Results range between 6.5 and 10 μmol/mol, which is much lower than the 100 μmol/mol threshold proposed by Boyle (1983) to sort out contaminated samples and eliminate trace element results that chiefly reflect the presence of oxides. Barker et al. (2003) also suggested that potential clay contamination should be checked for using an Al/Ca < 0.5 mmol/mol. All Al/Ca results are below 0.2 mmol/mol, thus indicating that the samples were well cleaned and free of sedimentary clay contamination.

Mg/Ca, Sr/Ca, Li/Ca, and U/Ca ratios for MD77-191 range from 0.5–1.5 mmol/mol, 0.8–2.1 mmol/mol, 2.7–6.4 μmol/mol, and 7.4–34.1 nmol/mol, respectively (Figures 3a–3d). All of these elemental ratios display a minimum during the 17–15.2 cal kyr BP time interval, with average values of ~0.8 mmol/mol for Mg/Ca, ~1.4 mmol/mol for Sr/Ca, ~3.9 μmol/mol for Li/Ca, and ~15.1 nmol/mol for U/Ca. Elemental ratios display higher values in the 15–13.3 cal kyr BP interval, and the most enriched values of Mg/Ca (1.5 mmol/mol), Sr/Ca (2.1 mmol/mol), Li/Ca (6.4 μmol/mol), and U/Ca (34.1 nmol/mol) occur during the same time interval. Thereafter, the Mg/Ca and Sr/Ca records generally show a continuous decrease throughout the deglaciation until the late Holocene. However, the continuous decrease is interrupted by an increase during the early Holocene (10.3–9 cal kyr BP). The lowest values are found in the late Holocene with mean values of Mg/Ca and Sr/Ca reaching 0.6 and 1.0 mmol/mol, respectively. The Li/Ca and U/Ca values also display a decreasing trend during the 12.6–10.5 cal kyr BP. U/Ca reaches its most depleted value (7.4 nmol/mol) at 10.8 cal kyr BP and then displays a significant increase during the early Holocene (10.3–9 cal kyr BP). Thereafter, lower values of Li/Ca and U/Ca (mean value of 3.5 μmol/mol and 17.3 nmol/mol, respectively) occurred during the 8.8–1.3 cal kyr BP time interval.

For Core MD77-176 from the BoB, Mg/Ca and Sr/Ca values for *H. elegans* range between 0.35 and 0.82 mmol/mol and between 0.55 and 1.32 mmol/mol, respectively. The *H. elegans* Mg/Ca and Sr/Ca records from MD77-176 show strong covariations (Figures 3e and 3f). The mean values of Mg/Ca (0.65 mmol/mol) and Sr/Ca (0.85 mmol/mol) during the LGM (22–17 cal kyr BP) are slightly higher compared with the Holocene (average values for Mg/Ca of 0.47 mmol/mol and for Sr/Ca of 0.72 mmol/mol). From 17 to about 12.5 cal kyr BP, the Mg/Ca and Sr/Ca records exhibit a succession of oscillations with a first minimum (0.39 and 0.7 mmol/mol, respectively) occurring between 17 and 15.4 cal kyr BP and a second shorter low (0.54 and 0.68 mmol/mol, respectively) between 13.4 and 12.5 cal kyr BP. In addition, during the last deglaciation period, the records display higher values (0.59 mmol/mol for Mg/Ca and 1.03 mmol/mol for Sr/Ca) at around 14.6 cal kyr BP, and the most enriched Mg/Ca (0.82 mmol/mol) and Sr/Ca (1.32 mmol/mol) values occur at the end of the last deglaciation (11.7–11.5 cal kyr BP). Then, during the Holocene, the values of Mg/Ca and Sr/Ca decrease continuously to reach a minimum (Mg/Ca for 0.35 mmol/mol and Sr/Ca for 0.55 mmol/mol) at the end of Holocene.

6. Discussion

Stable isotopes and elemental ratio records obtained for benthic foraminifera from Cores MD77-176 and MD77-191 show significant changes from the last deglaciation to the Holocene, as well as millennial-scale events. To better understand these variations, we compare our records with those from other areas and use the geochemical proxies to calculate different intermediate water mass parameters such as temperature and $[CO_3^{2-}]$. Moreover, since all proxies seem to follow the same trends, it is quite challenging to identify the main environmental control on each of them; thus, the limitations of these proxies are also discussed.

6.1. Assessing Past Variations in Intermediate Water Temperature

On the evidence of previous works, the environmental controls on benthic foraminiferal elemental ratios are not always well understood. For instance, the U/Ca of both calcitic benthic and planktonic foraminifera shows a negative correlation with $[CO_3^{2-}]$ (e.g., Keul et al., 2013; Raitzsch et al., 2011; Russell

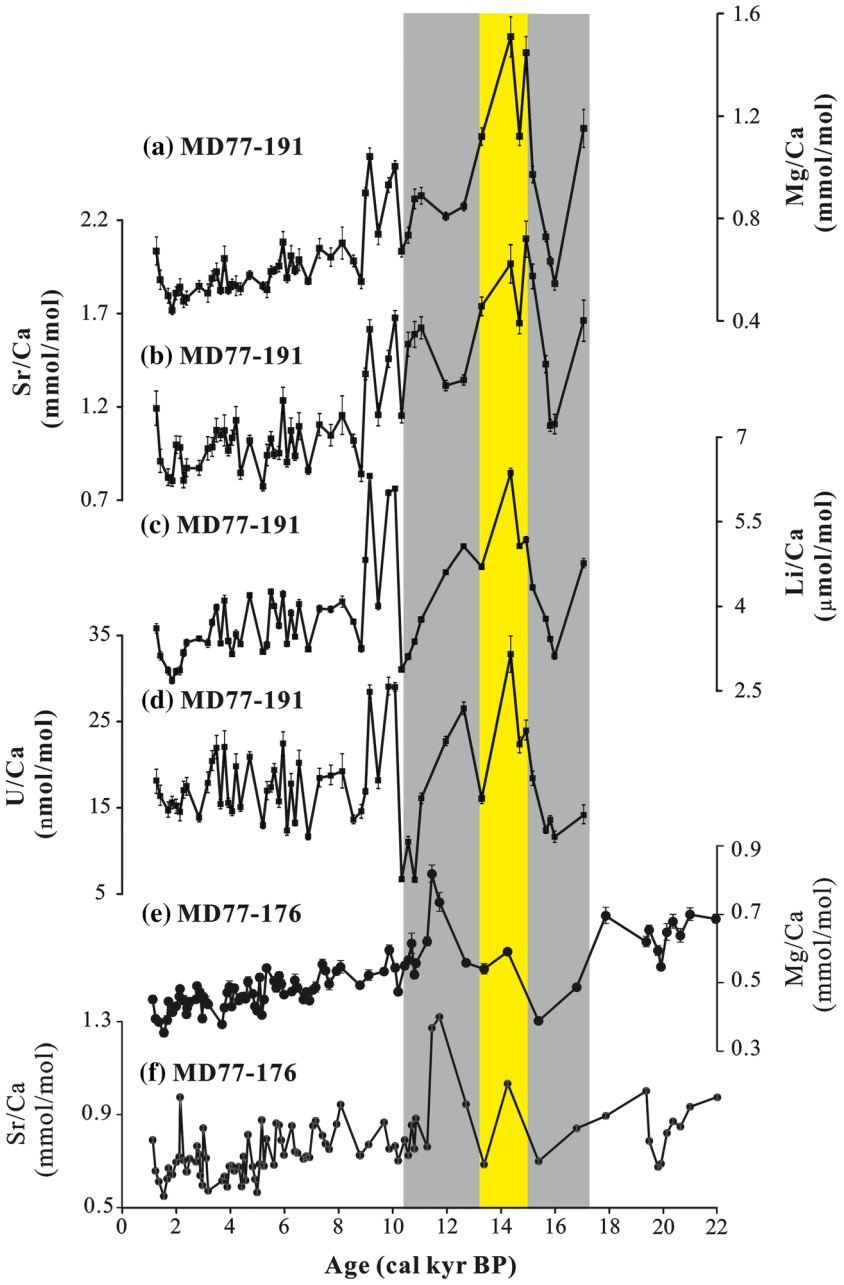

Figure 3. Comparison of benthic foraminifera *H. elegans* elemental ratios. (a–d) MD77-191 Mg/Ca, Sr/Ca, Li/Ca, and U/Ca; (e and f) MD77-176 Mg/Ca and Sr/Ca. The color-shaded intervals are the same as in Figure 2.

et al., 2004), whereas Chen et al. (2017) indicated that there is no significant correlation between calcitic benthic U/Ca and carbonate system parameters. Furthermore, as *H. elegans* is an aragonitic species, we cannot discard the influence of temperature on this proxy (Chen et al., 2017; Keul et al., 2013; Raitzsch et al., 2011). Thus, due to the difficulty to interpret properly this proxy, we preferred not to include the results in the discussion.

For the other elemental ratios, based on several studies carried out on aragonite benthic species *H. elegans*, Rosenthal et al. (2006) proposed that the Mg/Ca and Sr/Ca of *H. elegans* may reflect a combination effect of $[CO_3^{2-}]$ and bottom water temperature when the degree of $\Delta[CO_3^{2-}]$ is below 15 μmol/mol. The Li/Ca ratio from both calcite and aragonite benthic species also seems to reflect changes in the $[CO_3^{2-}]$ saturation state and bottom paleotemperature (Hall & Chan, 2004; Lear et al., 2010; Lear & Rosenthal, 2006; Marchitto

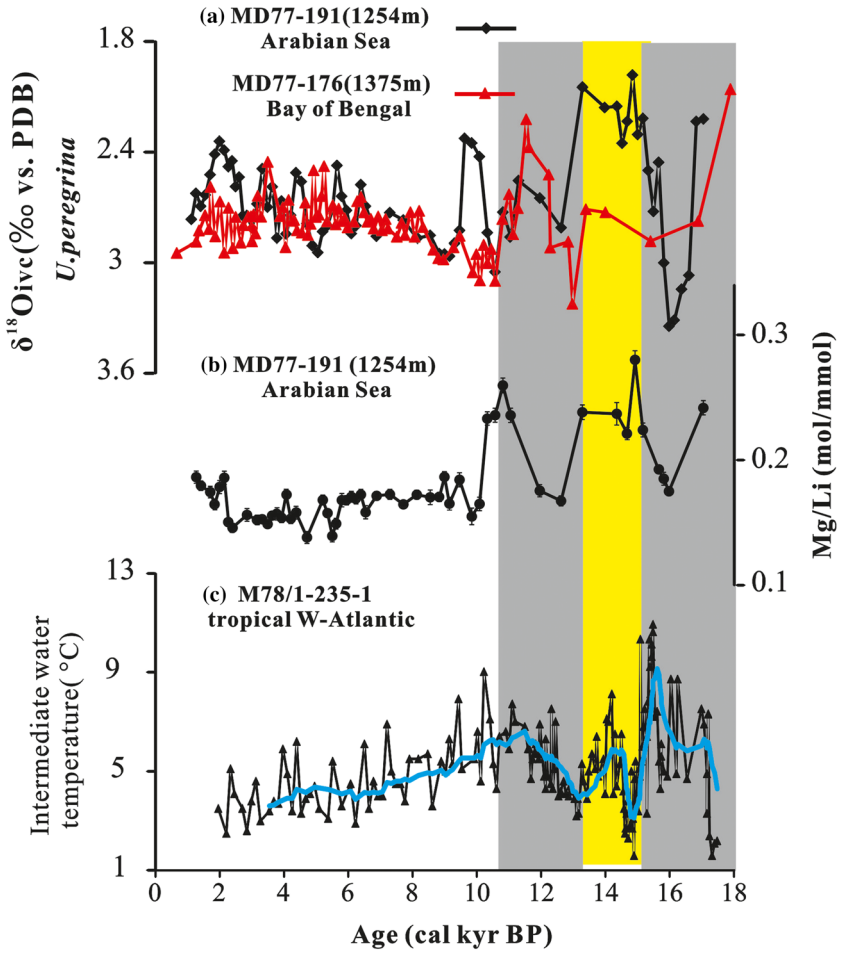

Figure 4. (a) Benthic $\delta^{18}O_{ivc}$ obtained from MD77-176 (Bay of Bengal; red line) and MD77-191 (Arabian Sea; black line), respectively. The benthic $\delta^{18}O_{ivc}$ is corrected by using the global ice volume $\delta^{18}O$. (b) *H. elegans* Mg/Li ratios obtained from MD77-191. (c) IWT record based on the $Mg/Ca_{Uvigerina}$ obtained from M78/1-235-1 in the tropical West Atlantic Ocean (Poggemann et al., 2018); the blue line is the smoothed curves using a 10-point average. The color-shaded intervals are the same as in Figure 2.

et al., 2004). However, as already observed in previous studies (Bryan & Marchitto, 2008; Marchitto et al., 2018), and in contrast to the Mg/Ca and Li/Ca ratios of *H. elegans*, the Mg/Li ratio shows a better correlation to bottom temperature. Thus, we decided to calculate the Mg/Li ratio from MD77-191 as a proxy for past intermediate water temperature (IWT). The Mg/Li values range between 0.14 and 0.28 mol/mmol (Figure 4b). However, according to the calibration published by Marchitto et al. (2018), this range of values corresponds to the coldest part of the equation, for which the Mg/Li ratio is less sensitive compared to the higher values. We observe that the Mg/Li values we calculated are in the lower range of the published results (Marchitto et al., 2018), but when we compare the Mg/Ca and Li/Ca of MD77-191 to the values from the same species *H. elegans* found in the literature (Mg/Ca and Li/Ca range from 0.5–1.7 mmol/mol and 1.4–9.3 μmol/mol, respectively; Bryan & Marchitto, 2008; Marchitto et al., 2018), results are in agreement. Thus, this observation gives us confidence to the Mg/Li ratios we calculated, despite a low range of values, maybe indicating small variations in the coldest range of the observed values. Therefore, rather than trying to calculate IWT values, it seems that the Mg/Li raw data are a reasonable reflection of variations in the IWT from MD77-191.

The *H. elegans* Mg/Li record shows decreasing trends during the 17–15.2 and 12.6–11.9 cal kyr BP time intervals; however, it displays higher values in the 15–13.3 cal kyr BP period. This may indicate colder IWT at the beginning and the end of the last deglaciation, compared to the 15–13.3 cal kyr BP (Figure 4b). Another significant increase in the Mg/Li ratio is observed at around 11–10.3 cal kyr BP, followed by stable and low

values during the Holocene. During the last deglaciation, previous studies have indicated an enhanced northward flow of AAIW in both the Atlantic and Indian Oceans (e.g., Bryan et al., 2010; Ma et al., 2019; Pahnke et al., 2008; Poggemann et al., 2017, 2018), suggesting that the source of intermediate water masses could at least partly be the same in both oceans. To test this hypothesis, we can compare the *H. elegans* Mg/Li results from MD77-191 with another IWT record obtained from the tropical West Atlantic Ocean, calculated using *Uvigerina* spp. Mg/Ca ratios (Core M78/1-235-1, 11°36.53′N–60°57.86′W, 852 m water depth; Poggemann et al., 2018; Figures 4b and 4c). Despite a higher resolution for M78/1-235-1 compared to MD77-191, both records seem to exhibit some similar trends, at least for the last 15.2 cal kyr BP. To better highlight these patterns, we compare the smoothed curve of M78/1-235-1 in the tropical West Atlantic Ocean with the MD77-19 record. Both records display an increasing trend centered at 14 cal kyr BP, followed by decreased values at around 13.3–11.9 cal kyr BP, and then a rise from about 11 to 10.3 kyr. The same trend in decreasing values can be observed over the Holocene (Figure 4).

In order to assess the validity of this reconstruction, benthic foraminiferal $\delta^{18}O$ can be used, since it records changes in global ice volume, local temperature, and, potentially, salinity. We used the ice volume-related, global seawater $\delta^{18}O$ estimate provided by Bintanja and van de Wal (2008) to correct the benthic $\delta^{18}O$ record for ice volume changes for both Cores MD77-191 and MD77-176. Thus, the resulting corrected $\delta^{18}O_{ivc}$ records indicate variations in both deepwater paleotemperature and/or salinity. In order to constrain past changes in the salinity, we can compare both core sites in the modern ocean. Indeed, the RSOW flows through a much stronger western boundary toward the Agulhas compared with eastward flows to the eastern boundary at 5°N (Beal et al., 2000; Talley et al., 2011; You, 1998). Thus, the site of MD77-191 (located in the eastern Arabian Sea) may be influenced by the RSOW, which is characterized by high salinity (Beal et al., 2000; Talley et al., 2011). However, the site of MD77-176 in the northeastern BoB should show little or no influence from the RSOW (Talley et al., 2011). Thus, the comparison between the $\delta^{18}O_{ivc}$ records obtained from MD77-176 and MD77-191 could reflect the influence of high-salinity RSOW (Figure 4a).

At the site of MD77-176, past IWT is more difficult to assess, as the benthic $\delta^{18}O_{ivc}$ was the only proxy used to reconstruct the past IWT. However, some similar trends are observed between the benthic $\delta^{18}O_{ivc}$ from MD77-176 and MD77-191. For the benthic $\delta^{18}O_{ivc}$ records obtained from these two cores, more enriched benthic $\delta^{18}O_{ivc}$ values (3.34‰ and 2.88‰, respectively) occurred during the 17–15.2 and 12.6–11.9 cal kyr BP time intervals, corresponding to colder and/or saltier deep water, and more depleted values (1.98‰ and 2.7‰, respectively) related to warmer and/or fresher deep water in the 15–13.3 cal kyr BP interval (Figure 4a). These trends match well with the MD77-191 *H. elegans* Mg/Li record at these time intervals, which may indicate cold IWT. By contrast, an increased trend in the Mg/Li ratio occurred at around 11–10.3 cal kyr BP, in opposition to the benthic $\delta^{18}O_{ivc}$ (Figures 4a and 4b). Differences are also observed during the Holocene, which could be related to past changes in the local salinity recorded in the benthic $\delta^{18}O_{ivc}$.

Thus, past IWT seem to have changed from the last deglaciation to the Holocene in the Arabian Sea, in the BoB, and in the tropical Atlantic, with the incursion of cold water masses at 17–15.2 and 12.6–11.9 cal kyr BP and two warmer events at 15–13.3 and 11–10.3 cal kyr BP. Furthermore, the $\delta^{18}O_{ivc}$ records obtained from MD77-176 and MD77-191 all display depleted values associated with warm and/or freshwater masses at 15–13.3 cal kyr BP during the last deglaciation, suggesting limited/no contribution of RSOW at the studied sites.

Then, a global trend to colder IWT is observed from the Mg/Li ratios across the Holocene, whereas both $\delta^{18}O_{ivc}$ records exhibit an opposite trend that may instead reflect the influence of fresher water masses. During the Holocene, increased benthic $\delta^{13}C$ and B-P age offsets obtained from MD77-176 in the BoB are synchronous with depleted ϵ_{Nd} records, suggesting the increased influence of NADW (Ma et al., 2019; Yu et al., 2018). All these records seem to indicate a limited influence of RSOW at both core sites during the Holocene, rather indicating an increased contribution of NADW (Ma et al., 2019; Yu et al., 2018).

However, during last deglaciation, colder water masses at 17–15.2 and 12.6–11.9 cal kyr BP in the North Indian Ocean seem to be inconsistent with previous studies suggesting a warming of AAIW during Heinrich Stadial 1 and Younger Dryas (Poggemann et al., 2018). This appearing discrepancy may relate to a smaller range of IWT variations in the northern Indian Ocean compared to other areas and/or to differences associated to local effects on the two areas that are very different. Thus, after having explored the past variations of IWT to track past intermediate water circulation changes, we investigate another important parameter, $[CO_3^{2-}]$.

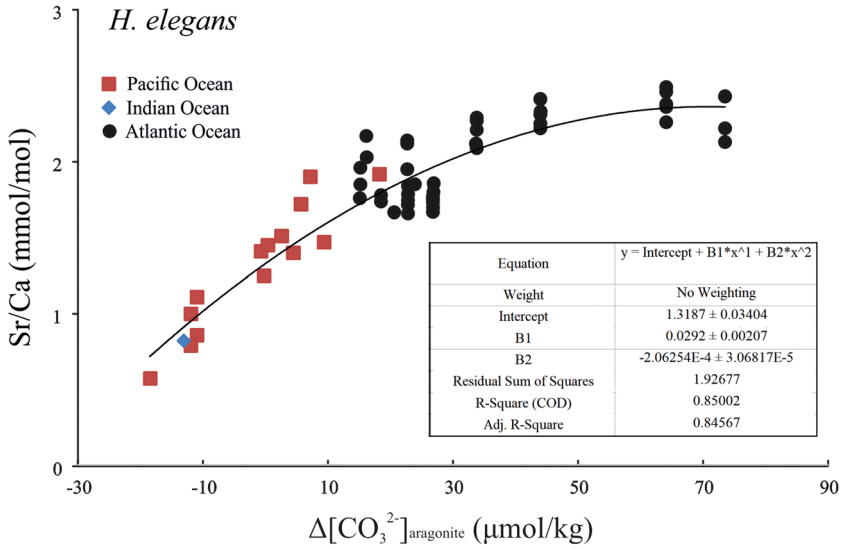

Figure 5. Core-top *H. elegans* Sr/Ca versus deepwater $\Delta[CO_3^{2-}]_{aragonite}$ (Rosenthal et al., 2006; Yu, Elderfield, et al., 2014).

6.2. Reconstructing Past Changes in the Intermediate Water $[CO_3^{2-}]$

6.2.1. Calculation of Past $[CO_3^{2-}]$

According to previous studies by Rosenthal et al. (2006) and, more recently, by Yu, Elderfield, et al. (2014), the *H. elegans* Sr/Ca values seem to covary with the bottom water $\Delta[CO_3^{2-}]$. The $\Delta[CO_3^{2-}]$ is defined as $\Delta[CO_3^{2-}] = [CO_3^{2-}] - [CO_3^{2-}]_{sat}$, where $[CO_3^{2-}]$ is carbonate ion and $[CO_3^{2-}]_{sat}$ is aragonite saturation concentration. The calculation of $[CO_3^{2-}]_{sat}$ at the studied sites was carried out using CO_2sys.xls (Ver. 12) (Pelletier et al., 2005). However, Rosenthal et al. (2006) have suggested that the *H. elegans* Sr/Ca is less sensitive to the $\Delta[CO_3^{2-}]_{aragonite}$ variations when values are above 15 μmol/mol. Yu, Elderfield, et al. (2014) summarized the published Sr/Ca calibration data for *C. wuellerstorfi*, *Cibicidoides mundulus*, *Uvigerina* spp., and *H. elegans*. Although not yet tested thoroughly, they proposed that the benthic Sr/Ca may be used as an auxiliary proxy for seawater $\Delta[CO_3^{2-}]$. To complete this approach, we collected the published core-top data for $\Delta[CO_3^{2-}]_{aragonite}$ paired with *H. elegans* Sr/Ca at intermediate water depth (500–1,500 m) (Rosenthal et al., 2006; Yu, Elderfield, et al., 2014) and plotted all of these Sr/Ca values together. Our database shows a positive relationship between Sr/Ca and bottom water $\Delta[CO_3^{2-}]_{aragonite}$ defined as follows: $Sr/Ca = -0.0002 \pm 0.00003\ \Delta[CO_3^{2-}]^2_{aragonite} + 0.0292 \pm 0.00207\ \Delta[CO_3^{2-}]_{aragonite} + 1.3187 \pm 0.03404$ ($r^2 = 0.85$) (Figure 5). The standard error of $\Delta[CO_3^{2-}]$ estimation from the Sr/Ca according to the determined equation is ±1 μmol/kg at −18.5 μmol/kg and ±7 μmol/kg at 74 μmol/kg. Thus, we calculated the intermediate water $\Delta[CO_3^{2-}]$ from the *H. elegans* Sr/Ca by using this equation. The seawater $[CO_3^{2-}]_{sat}$ is mainly affected by salinity, temperature, and water depth (pressure), for which variations on glacial-interglacial timescales are about ±0.5 μmol/kg, remaining roughly unchanged in the deep ocean (Yu et al., 2008; Yu, Anderson, et al., 2014). Therefore, it is possible to get the paleo-$[CO_3^{2-}]$ of the intermediate water at our core sites, thanks to the equation defined above and assuming little changes in the seawater $[CO_3^{2-}]_{sat}$.

The reconstructed intermediate water $[CO_3^{2-}]$ at the site of MD77-191 displays a decreasing trend during the 17–15.2 and 12.6–10.5 cal kyr BP time intervals, ranging between 97 and 77 μmol/kg and between 95 and 84 μmol/kg, respectively. The $[CO_3^{2-}]$ concentrations reach maximum values (~119 μmol/kg) in the 15–13.3 cal kyr BP. During the early Holocene (10.3–9 cal kyr BP), mean values are about 87 μmol/kg, and then we observed lower values of ~67 μmol/kg during the late Holocene (8.8–1.3 cal kyr BP).

The record of intermediate water $[CO_3^{2-}]$ at the site of MD77-176 shows slightly higher values during the LGM (~71 μmol/kg) than during the Holocene (~68 μmol/kg). For the period of the last deglaciation, the intermediate water $[CO_3^{2-}]$ record displays a decreasing trend to around ~67 μmol/kg at the 17–15.2 cal kyr BP interval and reaches a value of about ~77 μmol/kg at 14.6 cal kyr BP. An increasing trend is

observed from 13.4 to 11.7–11.5 cal kyr BP, with two extreme high values of 84–86 μmol/kg. Then, a global decrease in the $[CO_3^{2-}]$ is recorded during the Holocene.

6.2.2. Possible Controls on $[CO_3^{2-}]$ Records

On the basis of approximation, $[CO_3^{2-}] \approx 0.6 \times (ALK - DIC)$ (Yu et al., 2016), and thus, carbonate ion concentration in the seawater reflects the balance between mechanisms that affect changes in alkalinity (ALK) and total DIC. These mechanisms are varied, and the most important ones involve biological regeneration, changes in the water mass sources, and/or mixing of different water masses and air-sea exchanges (Yu et al., 2008). Deep water $[CO_3^{2-}]$ affects the dissolution/preservation of $CaCO_3$ on the seafloor by determining the seawater carbonate saturation and therefore acts as a control on the global oceanic ALK inventory (Yu, Anderson, et al., 2014).

Biological regeneration is linked to the sinking of organic matter and $CaCO_3$. The remineralization of sinking organic matter releases CO_2 in the deep ocean (Holligan & Robertson, 1996; Yu et al., 2008). The released CO_2 will consume $[CO_3^{2-}]$ to produce bicarbonate ions (HCO_3^-), resulting in a decrease in carbonate ions (Holligan & Robertson, 1996). Thus, the ratio of organic to inorganic carbon (the so-called rain ratio) has an important effect on the $[CO_3^{2-}]$ concentration; an increasing rain ratio leads to the reduction of the $[CO_3^{2-}]$ concentration of the deep ocean (Berger & Keir, 1984; Holligan & Robertson, 1996; Yu et al., 2008).

At the location of MD77-191, paleoproductivity is controlled by summer monsoon upwelling activity. An abundance of *G. bulloides* identified in Cores MD77-191 and SK237 GC04 (10°58.65′N–74°59.96′E, 1,245 m water depth) indicates a progressive increase of surface productivity during the Holocene, with a significant increase since ~6 cal kyr BP (Bassinot et al., 2011; Naik et al., 2017; Figure 6). In addition, the total organic carbon (C_{org}) can be used as an indicator of paleoproductivity (e.g., Calvert et al., 1995; Naidu et al., 1992). The C_{org} record obtained from SK237 GC04 also shows an increasing trend during the late Holocene and reaches a maximum value at the end of the Holocene (Figure 6). An increasing rain ratio (more organic matter sinking) caused a decreased $[CO_3^{2-}]$ concentration in the deep ocean (Berger & Keir, 1984; Holligan & Robertson, 1996; Yu et al., 2008; Yu et al., 2019). In addition, a decrease in the $[CO_3^{2-}]$ concentration is observed, which is consistent with high productivity during the Holocene (8.8–1.3 cal kyr BP). This hypothesis is also supported by the benthic Cd/Ca record from MD77-191 as a proxy to reconstruct the paleonutrient concentration of the intermediate water (unpublished data). Thus, we suggest that at the site of Core MD77-191, changes in the paleoproductivity resulting from the progressive increase of upwelling activity have involved an increase in organic matter rain and a depletion of $[CO_3^{2-}]$.

However, at the site of Core MD77-176 in the northern BoB, primary productivity is much lower than in the Arabian Sea in modern times and may not have a strong influence on the intermediate water $[CO_3^{2-}]$. Indeed, the modern distribution of chlorophyll in the surface water of the northeastern BoB indicates a slight increase in productivity during the winter monsoon (O'Malley, 2017; Thushara & Vinayachandran, 2016), and to our knowledge, there is no paleorecord of primary productivity in this area. Moreover, the paleosurface productivity in the BoB is much lower compared to the Arabian Sea (Prasanna Kumar et al., 2001). Thus, assuming that changes in primary productivity since the last deglaciation may not have been as strong as in the Arabian Sea, indicating less organic matter sinking from the surface, we suggest that paleoproductivity does not appear to be a major control in affecting the variation of $[CO_3^{2-}]$ concentrations in the northeastern BoB.

In addition, in order to examine the variations at a millennial timescale since the last deglaciation at intermediate and deepwater depth from a global view, we compared the seawater $[CO_3^{2-}]$ records from MD77-191 and MD77-176 with $[CO_3^{2-}]$ results reconstructed from the benthic foraminiferal B/Ca at different water depths from the Atlantic Ocean (BOFS 17K, 58.0°N–16.5°E, 1,150 m water depth) and the Indian Ocean (WIND 28K, 10.2°S–51.8°E, 4,147 m water depth) (Yu et al., 2008; Yu, Broecker, et al., 2010) (Figure 6). Similar trends are observed during the Holocene, with lower values recorded throughout these locations (Figure 6). This global decrease is likely to result from a depletion in the oceanic ALK (Yu, Anderson, et al., 2014), since we know that reducing the whole ocean ALK inventory may decrease the CO_2 solubility, thus driving up the atmospheric CO_2 over the last 8 cal kyr BP (Menviel & Joos, 2012; Ridgwell et al., 2003; Yu, Anderson, et al., 2014). In addition, the decreased $[CO_3^{2-}]$ during the Holocene could also be associated with increased coral reef construction due to the higher sea level, which could

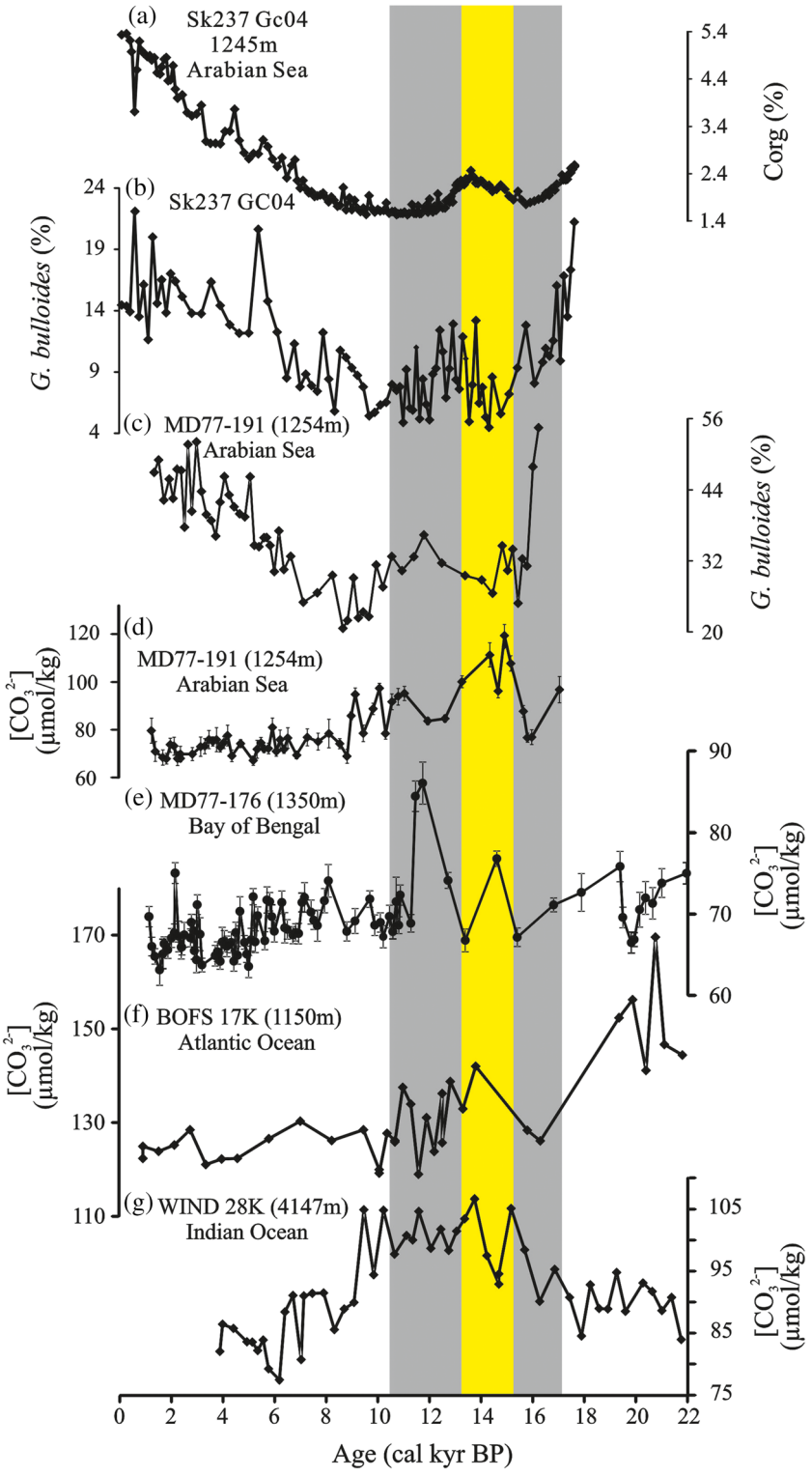

Figure 6. (a) The total organic carbon percentage ($\%C_{org}$) and (b) *G. bulloides* percentage from Core SK237 GC04 (1,245 m, Naik et al., 2017). (c) The relative abundance of *G. bulloides* and (d–g) comparison between $[CO_3^{2-}]$ records obtained from studied Cores MD77-191 (Arabian Sea) and MD77-176 (Bay of Bengal) with other $[CO_3^{2-}]$ records at different depths in the Indian Ocean and Atlantic Ocean (Yu et al., 2008; Yu, Broecker, et al., 2010). The color-shaded intervals are the same as in Figure 2.

remove the global ALK and induce a decline in $[CO_3^{2-}]$ over the whole ocean (Opdyke & Walker, 1992; Yu, Anderson, et al., 2014).

During the last deglaciation, the $[CO_3^{2-}]$ records at intermediate water depth from the Arabian Sea and the Atlantic Ocean display low values during the 17–15.2 and 12.6–10.5 kyr intervals. The record of intermediate $[CO_3^{2-}]$ obtained from MD77-176 closely matches previous records for the 17–15.2 cal kyr BP interval but, in contrast, displays maximum values (~84–86 μmol/kg) at 11.7–11.5 cal kyr BP, corresponding to a marked decrease trend of the benthic $\delta^{18}O$ (2.51‰) and benthic $\delta^{13}C$ (−0.19‰) at 11.5 cal kyr BP. Variations during this specific time interval thus seem to be associated with a local effect at the site of MD77-176, combining changes in the water mass salinity and/or temperature and $[CO_3^{2-}]$. Furthermore, the decrease of benthic $\delta^{13}C$ may correspond to the influenced discharge of terrigenous organic matter into the ocean, in a good agreement with the marked depleted benthic $\delta^{18}O$, which associated with warm and/or fresh water. Thus, this significant variation seems to be associated to the local large input of fresh water in the BoB. At the same time, in the deep Atlantic, equatorial Pacific, and Indian Oceans, deepwater $[CO_3^{2-}]$ concentrations rose by about ~10 μmol/kg (Yu et al., 2008; Yu, Anderson, et al., 2014; Yu, Broecker, et al., 2010; Yu, Foster, et al., 2010). The increased deepwater $[CO_3^{2-}]$ would have promoted deep-sea carbonate preservation and hence would have depleted the oceanic ALK inventory. Such an increase in deepwater $[CO_3^{2-}]$ concentration is coeval with the two-step deglacial increase of atmospheric CO_2 (Figure 7). This probably indicates that the deepwater carbonate ion increases results from a drop in DIC associated with the transfer of CO_2 from the deep ocean to the upper water depth and, ultimately, to the atmosphere. The release of deep-sea CO_2 may have induced a $[CO_3^{2-}]$ decline at intermediate depths (Yu, Anderson, et al., 2014). Such a hypothesis is consistent with the variations in intermediate $[CO_3^{2-}]$ concentration records from the northern BoB, Arabian Sea, and northern Atlantic Ocean (Figure 6).

6.3. Significance With Regard to Paleoclimate and Atmospheric CO_2 Changes

Comparing the paleo-$[CO_3^{2-}]$ records with other proxies, the decrease in $[CO_3^{2-}]$ records corresponds to an increase in benthic $\delta^{13}C$ during the last deglaciation. Such an increase in benthic $\delta^{13}C$ values has also been observed in previous studies from the northern Indian Ocean (e.g., Curry et al., 1988; Duplessy et al., 1984; Jung et al., 2009; Ma et al., 2019; Naqvi et al., 1994). This increase of benthic $\delta^{13}C$ in the Holocene may reflect more invigorated circulation associated with better-ventilated waters at intermediate depth in the northern Indian Ocean (Duplessy et al., 1984; Ma et al., 2019; Waelbroeck et al., 2006). The similarity of the benthic $\delta^{13}C$ increases reflects the northward expansion of AAIW during time intervals 17–15.2 and 12.6–10.5 cal kyr BP in the western Arabian Sea, Pacific Ocean, and BoB (Figure S3) (Jung et al., 2009; Ma et al., 2019; Pahnke & Zahn, 2005). However, as AAIW is formed from the deep waters of the AABW, air-sea exchange could also affect the values of $\delta^{13}C$, as the intermediate benthic $\delta^{13}C$ in the Southern Ocean is dominated by the influence of air-sea exchange (Lynch-Stieglitz et al., 1994). Thus, values for intermediate benthic $\delta^{13}C$ could increase relatively via stronger upwelling during the formation of AAIW. In addition, the transition in the ϵ_{Nd} and $\Delta^{14}C$ records during the deglaciation also indicates a strong northward penetration of AAIW within the North Atlantic and BoB (e.g., Cao et al., 2007; Ma et al., 2019; Pahnke et al., 2008; Pena et al., 2013; Yu et al., 2018). During the last deglaciation, MD77-176 B-P age offsets display a decreasing trend in the 17–15.2 and 12.6–10.5 cal kyr BP intervals, corresponding to increases in benthic $\delta^{13}C$ values (Figure 7). The variations in the B-P age offsets obtained from MD77-176 (northern BoB), Arabian Sea, and Pacific Ocean all indicate stronger upwelling and an enhanced northern flow of AAIW from the Southern Ocean during these two periods.

Therefore, during the 17–15.2 and 12.6–10.5 cal kyr BP intervals, changes in the benthic $\delta^{13}C$, B-P age offsets and ε_{Nd} records obtained from MD77-191 and MD77-176, associated to an increased atmospheric CO_2, could strongly support the hypothesis that enhanced vertical ventilation in the Southern Ocean could have led to an increased production of intermediate water masses (AAIW). As a consequence, enhanced Southern Ocean ventilation could have played an important role in the CO_2 increase during the last deglaciation (Anderson et al., 2009; Poggemann et al., 2017, 2018; Skinner et al., 2014).

In addition, as mentioned before, during the last deglaciation, the synchronicity of depleted intermediate water $[CO_3^{2-}]$ in the Indian and Atlantic Oceans increased deepwater $[CO_3^{2-}]$ in the global ocean (Yu

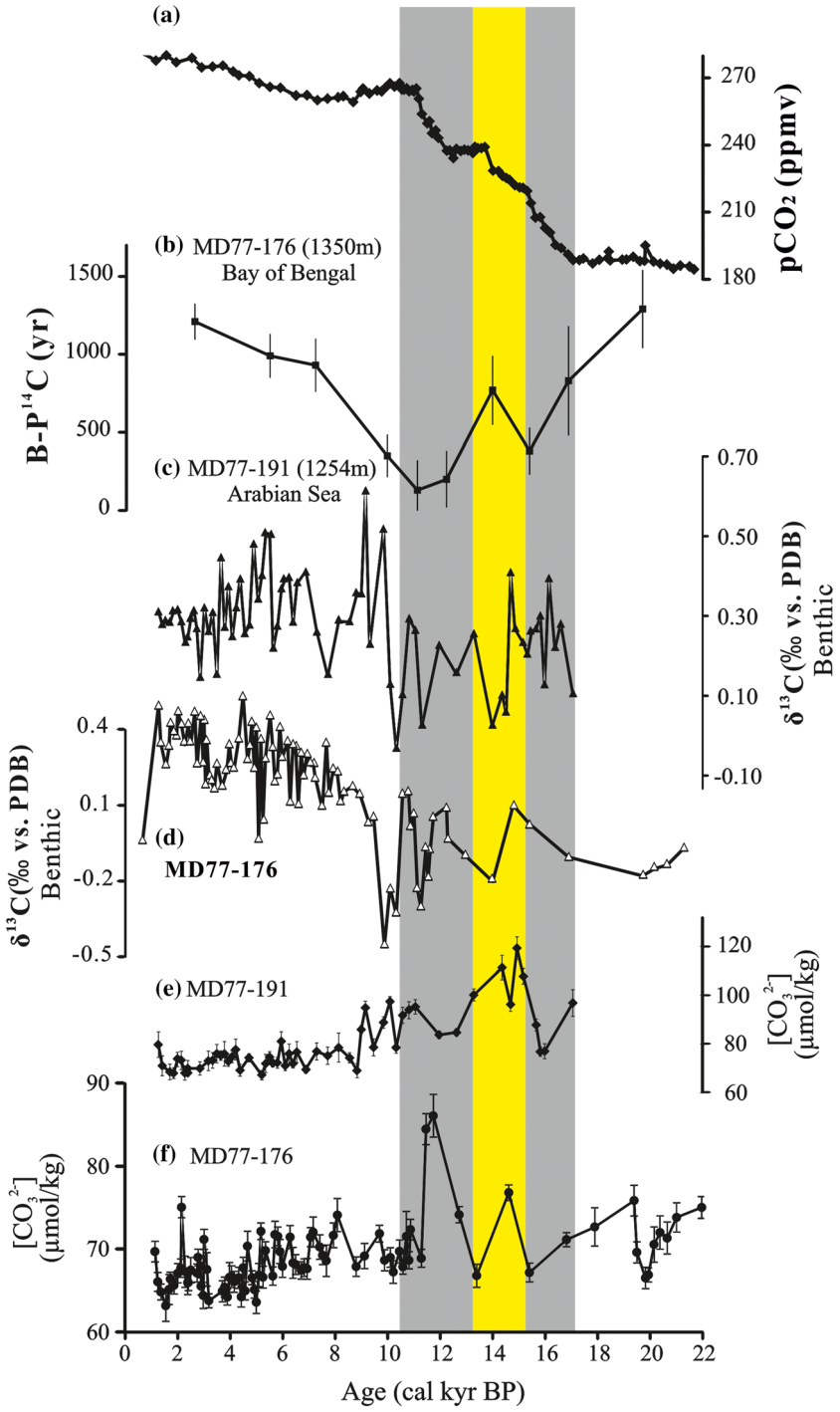

Figure 7. (a) Ice core atmospheric CO_2 from Antarctic Dome C (Monnin et al., 2001), (b) the intermediate water B-P ^{14}C age offset of MD77-176 in the BoB (Ma et al., 2019), (c and d) benthic $\delta^{13}C$ from studied Cores MD77-176 and MD77-191, respectively, and (e and f) compilation of $[CO_3^{2-}]$ records from Cores MD77-191 and MD77-176. The color-shaded intervals are the same as in Figure 2.

et al., 2008; Yu, Foster, et al., 2010; Yu, Broecker, et al., 2010; Yu, Anderson, et al., 2014), associated with the transfer of CO_2 from the deep ocean to the atmosphere (Yu, Anderson, et al., 2014). Thus, the depleted intermediate water $[CO_3^{2-}]$ could strongly support that variations of the Southern Ocean circulation contribute to these increases of atmospheric CO_2 by transferring the deep ocean carbon to the upper

ocean and atmosphere during the last deglaciation, by enhancing the upwelling and increasing the northward penetration of the AAIW in all ocean basins (e.g., Anderson et al., 2009; Jung et al., 2009; Ma et al., 2019; Pahnke & Zahn, 2005) at 17–15.2 and 12.6–10.5 cal kyr BP. In addition, the variations in intermediate-deepwater [CO_3^{2-}] are associated with the carbonate compensation and/or reef buildup due to increased sea level; these could confirm the influence of whole ocean ALK inventory in carbon reorganization in the Earth's biosphere system (Yu, Anderson, et al., 2014). Furthermore, for MD77-191 located in the south tip of India, the depleted intermediate water [CO_3^{2-}] during the Holocene may also be influenced by increased local paleoproductivity.

7. Conclusions

Benthic foraminifera $\delta^{13}C$, $\delta^{18}O$, and elemental ratios of *H. elegans* have been analyzed on Core MD77-191 (1,254 m water depth) located at the southern tip of India, as well as Core MD77-176 (1,375 m water depth) obtained from the northern BoB, to reconstruct the evolution of intermediate water masses in the northern Indian Ocean since the last deglaciation.

The past IWT in the northern Indian Ocean were mainly reconstructed using the *H. elegans* Mg/Li record obtained from MD77-191 in the Arabian Sea. It seems to indicate the influence of cold water mass during the last deglaciation (17–15.2 and 12.6–11.9 cal kyr BP time intervals) and a global trend toward colder IWT during the Holocene. In addition, two warmer events occurred at around 15–13.3 and 11–10.3 cal kyr BP time intervals.

We reconstructed seawater [CO_3^{2-}] concentration by converting *H. elegans* Sr/Ca to intermediate water [CO_3^{2-}] using a modern, core top-based, empirical relationship with the standard error of $\Delta[CO_3^{2-}] \pm 1$ μmol/kg at −18.5 μmol/kg and ±7 μmol/kg at 74 μmol/kg. During the last deglaciation, increased benthic $\delta^{13}C$, depletion in [CO_3^{2-}], and decreased B-P age offsets occurred in the 17–15.2 and 12.6–10.5 cal kyr BP intervals. All of these results suggest a strong linkage between Southern Ocean enhanced ventilation via AAIW and release of CO_2 during the last deglaciation. The decreased [CO_3^{2-}] in intermediate water masses also provides evidence for the important influence of variations in the global ALK inventory during the late Holocene, corresponding to the rise in atmospheric CO_2 since 8 kyr BP and/or increased productivity throughout the Holocene (at least for MD77-191).

Acknowledgments

The authors wish to thank the reviewers for useful suggestions and discussions during the revision process. The research was funded by the French National Research Agency (Agence Nationale de la Recherche) L-IPSL Project (Grant ANR-10-LABX-0018) and the INSU-LEFE-IMAGO-CITRON GLACE project. Data generated by this study are available at the PANGAEA database (https://doi.pangaea.de/10.1594/PANGAEA.916015). In addition, ICP-MS settings for elemental ratio determinations are given in Data Set S1.

References

Ahmad, S. M., Babu, A. G., Padmakumari, V. M., & Raza, W. (2008). Surface and deep water changes in the northeast Indian Ocean during the last 60 ka inferred from carbon and oxygen isotopes of planktonic and benthic foraminifera. *Palaeogeography Palaeoclimatology Palaeoecology*, *262*(3-4), 182–188. https://doi.org/10.1016/j.palaeo.2008.03.007

Ahmad, S. M., Zheng, H., Raza, W., Zhou, B., Lone, M. A., Raza, T., & Suseela, G. (2012). Glacial to Holocene changes in the surface and deep waters of the northeast Indian Ocean. *Marine Geology*, *329-331*, 16–23. https://doi.org/10.1016/j.margeo.2012.10.002

Anderson, R. F., Ali, S., Bradtmiller, L. I., Nielsen, S. H. H., Fleisher, M. Q., Anderson, B. E., & Burckle, L. H. (2009). Wind-driven upwelling in the Southern Ocean and the deglacial rise in atmospheric CO_2. *Science*, *323*(5920), 1443–1448. https://doi.org/10.1126/science.1167441

Barker, S., Greaves, M., & Elderfield, H. (2003). A study of cleaning procedures used for foraminiferal Mg/Ca paleothermometry. *Geochemistry, Geophysics, Geosystems*, *4*(9), 8407. https://doi.org/10.1029/2003GC000559

Barrientos, A., Lear, C. H., Jakobsson, M., Stranne, C., O'Regan, M., Cronin, T. M., et al. (2018). Arctic Ocean benthic foraminifera Mg/Ca ratios and global Mg/Ca-temperature calibrations: New constraints at low temperatures. *Geochimica et Cosmochimica Acta*, *236*, 240–259. https://doi.org/10.1016/j.gca.2018.02.036

Bassinot, F. C., Marzin, C., Braconnot, P., Marti, O., Mathienblard, E., Lombard, F., & Bopp, L. (2011). Holocene evolution of summer winds and marine productivity in the tropical Indian Ocean in response to insolation forcing: Data-model comparison. *Climate of the Past*, *7*(3), 815–829. https://doi.org/10.5194/cp-7-815-2011

Beal, L. M., Ffield, A., & Gordon, A. L. (2000). Spreading of Red Sea overflow waters in the Indian Ocean. *Journal of Geophysical Research*, *105*(C4), 8549–8564. https://doi.org/10.1029/1999JC900306

Berger, W. H., & Keir, R. S. (1984). Glacial-Holocene changes in atmospheric CO_2 and the deep-sea record. In J. E. Hansen & T. Takahashi (Eds.), *Climate processes and climate sensitivity* (pp. 337–351). Washington DC: AGU. https://doi.org/10.1029/GM029p0337

Bintanja, R., & van de Wal, R. S. W. (2008). North American ice-sheet dynamics and the onset of 100,000-year glacial cycles. *Nature*, *454*(7206), 869–872. https://doi.org/10.1038/nature07158

Boyle, E. A. (1983). Manganese carbonate overgrowths on foraminifera tests. *Geochimica et Cosmochimica Acta*, *63*(18), 353–353.

Boyle, E. A., & Keigwin, L. D. (1985). Comparison of Atlantic and Pacific paleochemical records for the last 215,000 years: Changes in deep ocean circulation and chemical inventories. *Earth and Planetary Science Letters*, *76*(1-2), 135–150. https://doi.org/10.1016/0012-821X(85)90154-2

Boyle, E. A., Labeyrie, L., & Duplessy, J. C. (1995). Calcitic foraminiferal data confirmed by cadmium in aragonite *Hoeglundina*: Application to the last glacial maximum in the northern Indian Ocean. *Paleoceanography*, *10*(5), 881–900. https://doi.org/10.1029/95PA01625

Broecker, W. S., & Peng, T.-H. (1982). *Tracers in the sea. Published by Lamont-Doherty Geological Observatory*, (p. 690). Columbia University, New York: Eldigio Press.

Brovkin, V., Ganopolski, A., Archer, D., & Rahmstorf, S. (2007). Lowering of glacial atmospheric CO_2 in response to changes in oceanic circulation and marine biogeochemistry. *Paleoceanography*, *22*, PA4202. https://doi.org/10.1029/2006PA001380

Bryan, S. P., & Marchitto, T. M. (2008). Mg/Ca–temperature proxy in benthic foraminifera: New calibrations from the Florida Straits and a hypothesis regarding Mg/Li. *Paleoceanography*, *23*, PA2220. https://doi.org/10.1029/2007PA001553

Bryan, S. P., Marchitto, T. M., & Lehman, S. J. (2010). The release of ^{14}C-depleted carbon from the deep ocean during the last deglaciation: Evidence from the Arabian Sea. *Earth and Planetary Science Letters*, *298*(1-2), 244–254. https://doi.org/10.1016/j.epsl.2010.08.025

Calvert, S. E., Pedersen, T. F., Naidu, P. D., & von Stackelberg, U. (1995). On the organic carbon maximum on the continental slope of the eastern Arabian Sea. *Journal of Marine Research*, *53*(2), 269–296. https://doi.org/10.1357/0022240953213232

Came, R. E., Oppo, D. W., Curry, W. B., & Lynch-Stieglitz, J. (2008). Deglacial variability in the surface return flow of the Atlantic meridional overturning circulation. *Paleoceanography*, *23*, PA1217. https://doi.org/10.1029/2007PA001450

Cao, L., Fairbanks, R. G., Mortlock, R. A., & Risk, M. J. (2007). Radiocarbon reservoir age of high latitude North Atlantic surface water during the last deglacial. *Quaternary Science Reviews*, *26*(5-6), 732–742. https://doi.org/10.1016/j.quascirev.2006.10.001

Chen, P. J., Yu, J., & Jin, Z. (2017). An evaluation of benthic foraminiferal U/Ca and U/Mn proxies for deep ocean carbonate chemistry and redox conditions. *Geochemistry, Geophysics, Geosystems*, *18*, 617–630. https://doi.org/10.1002/2016GC006730

Curry, W. B., Duplessy, J. C., Labeyrie, L. D., & Shackleton, N. J. (1988). Changes in the distribution of δ^{13}C of deep water σCO_2 between the last glaciation and the Holocene. *Paleoceanography*, *3*(3), 317–341. https://doi.org/10.1029/PA003i003p00317

Doss, W., Marchitto, T. M., Eagle, R., Rashid, H., & Tripati, A. (2018). Deconvolving the saturation state and temperature controls on benthic foraminiferal Li/Ca, based on downcore paired B/Ca measurements and coretop compilation. *Geochimica et Cosmochimica Acta*, *236*, 297–314. https://doi.org/10.1016/j.gca.2018.02.029

Duplessy, J.-C., Shackleton, N. J., Matthews, R. K., Prell, W., Ruddiman, W. F., Caralp, M., & Hendy, C. H. (1984). ^{13}C record of benthic foraminifera in the last interglacial ocean: Implications for the carbon cycle and the global deep water circulation. *Quaternary Research*, *21*(2), 225–243. https://doi.org/10.1016/0033-5894(84)90099-1

Goyet, C., Healy, R., Ryan, J., Kozyr, A. (2000). Global distribution of total inorganic carbon and total alkalinity below the deepest winter mixed layer depths. ORNL/CDIAC-127, 28 pp., Carbon Dioxide Inf. Anal. Cent., Oak Ridge Natl. Lab., Oak Ridge, Tenn.

Hall, J. M., & Chan, L.-H. (2004). Li/Ca in multiple species of benthic and plaktonic foraminifera: Thermocline, latitudinal, and glacial-interglacial variation. *Geochimica et Cosmochimica Acta*, *68*(3), 529–545. https://doi.org/10.1016/S0016-7037(03)00451-4

Holligan, P. M., & Robertson, J. E. (1996). Significance of ocean carbonate budgets for the global carbon cycle. *Global Change Biology*, *2*(2), 85–95. https://doi.org/10.1111/j.1365-2486.1996.tb00053.x

IPCC, 2013. Climate change 2013: The physical science basis summary for policymakers. Intergovernmental Panel on Climate Change.

Jung, S. J. A., Kroon, D., Ganssen, G., Peeters, F., & Ganeshram, R. (2009). Enhanced Arabian Sea intermediate water flow during glacial North Atlantic cold phases. *Earth and Planetary Science Letters*, *280*(1-4), 220–228. https://doi.org/10.1016/j.epsl.2009.01.037

Keul, N., Langer, G., Nooijer, L. J. D., Nehrke, G., Reichart, G. J., & Bijma, J. (2013). Incorporation of uranium in benthic foraminiferal calcite reflects seawater carbonate ion concentration. *Geochemistry, Geophysics, Geosystems*, *14*, 102–111. https://doi.org/10.1029/2012GC004330

Lear, C. H., Mawbey, E. M., & Rosenthal, Y. (2010). Cenozoic benthic foraminiferal Mg/Ca and Li/Ca records: Toward unlocking temperatures and saturation states. *Paleoceanography*, *25*, PA4215. https://doi.org/10.1029/2009PA001880

Lear, C. H., & Rosenthal, Y. (2006). Benthic foraminiferal Li/Ca: Insights into Cenozoic seawater carbonate saturation state. *Geology*, *34*(11), 985–988. https://doi.org/10.1130/G22792A.1

Lear, C. H., Rosenthal, Y., & Slowey, N. (2002). Benthic foraminiferal Mg/Ca-paleothermometry: A revised core-top calibration. *Geochimica et Cosmochimica Acta*, *66*(19), 3375–3387. https://doi.org/10.1016/S0016-7037(02)00941-9

Lisiecki, L., & Raymo, M. (2005). A Pliocene-Pleistocene stack of 57 globally distributed benthic ^{18}O records. *Paleoceanography*, *20*, PA1003 https://doi.org/10.1029/2004PA001071

Lüthi, D., Le Floch, M., Bereiter, B., Blunier, T., Barnola, J.-M., Siegenthaler, U., et al. (2008). High-resolution carbon dioxide concentration record 650,000–800,000 years before present. *Nature*, *453*(7193), 379–382. https://doi.org/10.1038/nature06949

Lutze, G. F., & Thiel, H. (1989). Epibenthic foraminifera from elevated microhabitats; *Cibicidoides wuellerstorfi* and *Planulina ariminensis*. *Journal of Foraminiferal Research*, *19*(2), 153–158. https://doi.org/10.2113/gsjfr.19.2.153

Lynch-Stieglitz, J., Fairbanks, R. G., & Charles, C. D. (1994). Glacial-interglacial history of Antarctic Intermediate Water: Relative strengths of Antarctic versus Indian Ocean sources. *Paleoceanography*, *9*(1), 7–29. https://doi.org/10.1029/93PA02446

Ma, R., Sépulcre, S., Licari, L., Bassinot, F., Liu, Z., Tisnérat-Laborde, N., et al. (2019). Changes in intermediate circulation in the Bay of Bengal since the Last Glacial Maximum as inferred from benthic foraminifera assemblages and geochemical proxies. *Geochemistry, Geophysics, Geosystems*, *20*, 1–17. https://doi.org/10.1029/2018GC008179

Mackensen, A., Hubberten, H. W., Bickert, T., Fischer, G., & Fütterer, D. K. (1993). The δ^{13}C in benthic foraminiferal tests of *Fontbotia wuellerstorfi* (Schwager) relative to the δ^{13}C of dissolved inorganic carbon in Southern Ocean Deep Water: Implications for glacial ocean circulation models. *Paleoceanography*, *8*(5), 587–610. https://doi.org/10.1029/93PA01291

Makou, M. C., Oppo, D. W., & Curry, W. B. (2010). South atlantic intermediate water mass geometry for the Last Glacial Maximum from foraminiferal Cd/Ca. *Paleoceanography*, *25*, PA4103. https://doi.org/10.1029/2010PA001962

Marchitto, C. S., Henderson, G. M., Crompoton, R., Staubwasser, M., & Shaw, S. (2004). Effect of mineralogy, salinity and temperature on Li/Ca and Li isotope composition of calcium carbonate. *Chemical Geology*, *212*, 5–15.

Marchitto, T. M., Bryan, S. P., Curry, W. B., & McCorkle, D. C. (2007). Mg/Ca temperature calibration for the benthic foraminifera *Cibicidoides pachyderma*. *Paleoceanography*, *22*, PA1203. https://doi.org/10.1029/2006PA001287

Marchitto, T. M., Bryan, S. P., Doss, W., Mcculloch, M., & Montagna, P. (2018). A simple biomineralization model to explain Li, Mg, and Sr incorporation into aragonitic foraminifera and corals. *Earth and Planetary Science Letters*, *481*, 20–29. https://doi.org/10.1016/j.epsl.2017.10.022

Martin, P. A., Lea, D. W., Rosenthal, Y., Shackleton, N. J., Sarnthen, M., & Papenfuss, T. (2002). Quaternary deep sea temperature histories derived from benthic foraminiferal Mg/Ca. *Earth and Planetary Science Letters*, *198*(1-2), 193–209. https://doi.org/10.1016/S0012-821X(02)00472-7

Marzin, C., Kallel, N., Kageyama, M., Duplessy, J. C., & Braconnot, P. (2013). Glacial fluctuations of the Indian monsoon and their relationship with North Atlantic climate: New data and modelling experiments. *Climate of the Past*, *9*(5), 2135–2151. https://doi.org/10.5194/cp-9-2135-2013

Menviel, L., & Joos, F. (2012). Toward explaining the Holocene carbon dioxide and carbon isotope records: Results from transient ocean carbon cycle-climate simulations. *Palaeogeogr. Palaeoclimatol. Palaeoecol*, *27*(PA1207), 1–17.

Mléneck, V. M. (1997). Sédimentation et dissolution des carbonates biogéniques aux moyennes latitudes Nord et Sud: approche quantitative et relations avec les paléocirculations océaniques des derniers 150.000 ans. PhD thesis, Universit'e Bordeaux I, pp. 277.

Monnin, E., Indermühle, A., Dällenbach, A., Flückiger, J., Stauffer, B., Stocker, T. F., et al. (2001). Atmospheric CO_2 concentrations over the last glacial termination. *Science*, *291*(5501), 112–114. https://doi.org/10.1126/science.291.5501.112

Naidu, P. D., Prakash Babu, C., & Rao, C. M. (1992). The upwelling record in the sediments of the western continental margin of India. *Deep Sea Research*, *39*(3-4), 715–723. https://doi.org/10.1016/0198-0149(92)90097-D

Naik, D. K., Saraswat, R., Lea, D. W., Kurtarkar, S. R., & Mackensen, A. (2017). Last glacial-interglacial productivity and associated changes in the eastern Arabian Sea. *Palaeogeography, Palaeoclimatology, Palaeoecology*, *483*, 147–156. https://doi.org/10.1016/j.palaeo.2016.07.014

Naqvi, W. A., Charles, C. D., & Fairbanks, R. G. (1994). Carbon and oxygen isotopic records of benthic foraminifera from the Northeast Indian Ocean: Implications on glacial-interglacial atmospheric CO_2 changes. *Earth and Planetary Science Letters*, *121*(1-2), 99–110. https://doi.org/10.1016/0012-821X(94)90034-5

O'Malley, R. (2017). Ocean productivity. http://www.science.oregonstate.edu/ocean.Produc-tivity/index.php

Opdyke, B. N., & Walker, J. C. G. (1992). Return of the coral reef hypothesis: Basin to shelf partitioning of $CaCO_3$ and its effect on atmospheric CO_2. *Geology*, *20*(8), 733–736. https://doi.org/10.1130/0091-7613(1992)020<0733:ROTCRH>2.3.CO;2

Pahnke, K., Goldstein, S. L., & Hemming, S. R. (2008). Abrupt changes in Antarctic Intermediate Water circulation over the past 25,000 years. *Nature Geoscience*, *1*(12), 870–874. https://doi.org/10.1038/ngeo360

Pahnke, K., & Zahn, R. (2005). Southern Hemisphere water mass conversion linked with North Atlantic climate variability. *Science*, *307*(5716), 1741–1746. https://doi.org/10.1126/science.1102163

Pelletier, G., Lewis, E., Wallace, D. (2005). A calculator for the CO_2 system in Seawater for Microsoft Excel/VBA. Washington State Department of Ecology, Olympia, WA, Brookhaven National Laboratory Upton, NY.

Pena, L. D., Goldstein, S. L., Hemming, S. R., Jones, K. M., Calvo, E., Pelejero, C., & Cacho, I. (2013). Rapid changes in meridional advection of Southern Ocean intermediate waters to the tropical Pacific during the last 30 kyr. *Earth and Planetary Science Letters*, *368*, 20–32. https://doi.org/10.1016/j.epsl.2013.02.028

Poggemann, D. W., Hathorne, E. C., Nürnberg, D., Frank, M., Bruhn, I., Reißig, S., & Bahr, A. (2017). Rapid deglacial injection of nutrients into the tropical Atlantic via Antarctic Intermediate Water. *Earth and Planetary Science Letters*, *463*, 118–126. https://doi.org/10.1016/j.epsl.2017.01.030

Poggemann, D.-W., Nürnberg, D., Hathorne, E. C., Frank, M., Rath, W., Reißig, S., & Bahr, A. (2018). Deglacial heat uptake by the Southern Ocean and rapid northward redistribution via Antarctic Intermediate Water. *Palaeogeography Palaeoclimatology Palaeoecology*, *33*(11), 1292–1305.

Prasanna Kumar, S., Madhupratap, M., Dileep Kumar, M., Muraleedharan, P. M., de Souza, S. N., Gauns, M., & Sarma, V. V. S. S. (2001). High biological productivity in the central Arabian Sea during the summer monsoon driven by Ekman pumping and lateral advection. *Current Science*, *81*, 1633–1638.

Raitzsch, M., Kuhnert, H., Hathorne, E. C., Groeneveld, J., & Bickert, T. (2011). U/Ca in benthic foraminifera: A proxy for the deep-sea carbonate saturation. *Geochemistry, Geophysics, Geosystems*, *12*, Q06019. https://doi.org/10.1029/2010GC003344

Ravichandran, M., Girishkumar, M. S., & Riser, S. (2012). Observed variability of chlorophyll-*a* using Argo profiling floats in the southeastern Arabian Sea. *Deep-Sea Research Part I*, *65*(65), 15–25. https://doi.org/10.1016/j.dsr.2012.03.003

Raza, T., Ahmad, S. M., Sahoo, M., Banerjee, B., Bal, I., Dash, S., et al. (2014). Hydrographic changes in the southern Bay of Bengal during the last ~65,000 y inferred from carbon and oxygen isotopes of foraminiferal fossil shells. *Quaternary International*, *333*, 77–85. https://doi.org/10.1016/j.quaint.2014.02.010

Reid, J. L. (2003). On the total geostrophic circulation of the South Pacific Ocean: Flow patterns, tracers and transports. *Progress in Oceanography*, *16*(1), 1–61.

Reimer, P. J., Bard, E., Bayliss, A., Beck, J. W., Blackwell, P. G., Bronk, R. C., et al. (2013). IntCal13 and Marine13 radiocarbon age calibration curves 0–50,000 years cal BP. *Radiocarbon*, *55*(4), 1869–1887. https://doi.org/10.2458/azu_js_rc.55.16947

Ridgwell, A., & Zeebe, R. E. (2005). The role of the global carbonate cycle in the regulation and evolution of the Earth system. *Earth and Planetary Science Letters*, *234*(3-4), 299–315. https://doi.org/10.1016/j.epsl.2005.03.006

Ridgwell, A. J., Watson, A. J., Maslin, M. A., & Kaplan, J. O. (2003). Implications of coral reef buildup for the controls on atmospheric CO_2 since the Last Glacial Maximum. *Paleoceanography*, *18*(4), 1083. https://doi.org/10.1029/2003PA000893

Rosenthal, Y., Boyle, E. A., & Slowey, N. (1997). Temperature control on the incorporation of magnesium, strontium, fluorine, and cadmium into benthic foraminiferal shells from little Bahama Bank: Prospects for thermocline paleoceanography. *Geochimica et Cosmochimica Acta*, *61*(17), 3633–3643. https://doi.org/10.1016/S0016-7037(97)00181-6

Rosenthal, Y., Lear, C. H., Oppo, D. W., & Linsley, B. K. (2006). Temperature and carbonate ion effects on Mg/Ca and Sr/Ca ratios in benthic foraminifera: Aragonitic species *Hoeglundina elegans*. *Paleoceanography*, *21*, PA1007. https://doi.org/10.1029/2005PA001158.

Russell, A. D., Honisch, B. H., Spero, J., & Lea, D. W. (2004). Effects of seawater carbonate ion concentration and temperature on shell U, Mg, and Sr in cultured planktonic foraminifera. *Geochimica et Cosmochimica Acta*, *68*(21), 4347–4361. https://doi.org/10.1016/j.gca.2004.03.013

Schlitzer, R. (2015). Ocean data view. http://odv.awi.de

Shackleton, N. J. (1974). Attainment of isotopic equilibrium between ocean water and benthonic foraminifera genus *Uvigerina*: Isotopic changes in the ocean during the last glacial. Les méthodes quantitatives d'étude des variations du climat au cours du pleistocène, Gif-Sur-Yvette. *Colloque international du CNRS 219*, 203–210.

Schott, F. A., & McCreary, J. P. (2001). The Monsoon Circulation of the Indian Ocean. *Progress In Oceanography*, *51*(1), 1–123. https://doi.org/10.1016/S0079-6611(01)00083-0

Sigman, D. M., & Boyle, E. A. (2000). Glacial/interglacial variations in atmospheric carbon dioxide. *Nature*, *407*(6806), 859–869. https://doi.org/10.1038/35038000

Sijinkumar, A. V., Clemens, S., Nath, B. N., Prell, W., Benshila, R., & Lengaigne, M. (2016). $\Delta^{18}O$ and salinity variability from the Last Glacial Maximum to recent in the Bay of Bengal and Andaman Sea. *Quaternary Science Reviews*, *135*, 79–91. https://doi.org/10.1016/j.quascirev.2016.01.022

Skinner, L. C., Waelbroeck, C., Scrivner, A. E., & Fallon, S. J. (2014). Radiocarbon evidence for alternating northern and southern sources of ventilation of the deep Atlantic carbon pool during the last deglaciation. *Proceedings of the National Academy of Sciences*, *111*(15), 5480–5484. https://doi.org/10.1073/pnas.1400668111

Stuiver, M., & Braziunas, T. F. (1993). Modeling atmospheric ^{14}C influences and ^{14}C ages of marine samples to 10,000 BC. *Radiocarbon*, *35*(1), 137–189. https://doi.org/10.1017/S0033822200013874

Talley, L. D., Pickard, G. L., Emery, W. J., & Swift, J. H. (2011). *Preface. In descriptive physical oceanography (sixth edition)*, (pp. 1–383). Boston: Academic Press.

Thushara, V., & Vinayachandran, P. N. (2016). Formation of summer phytoplankton bloom in the northwestern Bay of Bengal in a coupled physical-ecosystem model. *Journal of Geophysical Research: Oceans*, *121*, 8535–8550. https://doi.org/10.1002/2016JC011987

Tomczak, M., & Godfrey, J. S. (2003). *Regional oceanography: An introduction* (second, pp. 1–390). Delhi: Daya Publishing House.

Waelbroeck, C., Levi, C., Duplessy, J. C., Labeyrie, L., Michel, E., Cortijo, E., et al. (2006). Distant origin of circulation changes in the Indian Ocean during the last deglaciation. *Earth and Planetary Science Letters*, *243*(1-2), 244–251. https://doi.org/10.1016/j.epsl.2005.12.031

You, Y. (1998). Intermediate water circulation and ventilation of the Indian Ocean derived from water-mass contributions. *Journal of Marine Research*, *56*(5), 1029–1067. https://doi.org/10.1357/002224098765173455

You, Y., & Tomczak, M. (1993). Thermocline circulation and ventilation in the Indian Ocean derived from water mass analysis. *Deep-Sea Research Part I*, *40*(1), 13–56. https://doi.org/10.1016/0967-0637(93)90052-5

Yu, J., Anderson, R. F., & Rohling, E. J. (2014). Deep ocean carbonate chemistry and glacial-interglacial atmospheric CO_2 change. *Oceanography*, *27*(1), 16–25. https://doi.org/10.5670/oceanog.2014.04

Yu, J., Broecker, W., Elderfield, H., Jin, Z. D., McManus, J., & Zhang, F. (2010). Loss of carbon from the deep sea since the Last Glacial Maximum. *Science*, *330*(6007), 1084–1087. https://doi.org/10.1126/science.1193221

Yu, J., & Broecker, W. S. (2010). Comment on "Deep-sea temperature and ice volume changes across the Pliocene-Pleistocene climate transitions". *Science*, *328*, 1480c. https://doi.org/10.1126/science.1186544

Yu, J., Day, J., Greaves, M., & Elderfield, H. (2005). Determination of multiple element/calcium ratios in foraminiferal calcite by quadrupole ICP-MS. *Geochemistry, Geophysics, Geosystems*, *6*, Q08P01. https://doi.org/10.1029/2005GC000964

Yu, J., & Elderfield, H. (2008). Mg/Ca in the benthic foraminifera *Cibicidoides wuellerstorfi* and *Cibicidoides mundulus*: Temperature versus carbonate ion saturation. *Earth and Planetary Science Letters*, *276*(1-2), 129–139. https://doi.org/10.1016/j.epsl.2008.09.015

Yu, J., Elderfield, H., Jin, Z., Tomascak, P., & Rohling, E. J. (2014). Controls on Sr/Ca in benthic foraminifera and implications for seawater Sr/Ca during the late Pleistocene. *Quaternary Science Reviews*, *98*(15), 1–6. https://doi.org/10.1016/j.quascirev.2014.05.018

Yu, J., Elderfield, H., & Piotrowski, A. M. (2008). Seawater carbonate ion-$\delta^{13}C$ systematics and application to glacial-interglacial North Atlantic Ocean circulation. *Earth and Planetary Science Letters*, *271*(1-4), 209–220. https://doi.org/10.1016/j.epsl.2008.04.010

Yu, J., Foster, G. L., Elderfield, H., Broecker, W. S., & Clark, E. (2010). An evaluation of benthic foraminiferal B/Ca and $\delta^{11}B$ for deep ocean carbonate ion and pH reconstructions. *Earth and Planetary Science Letters*, *293*(1-2), 114–120. https://doi.org/10.1016/j.epsl.2010.02.029

Yu, J., Menviel, L., Jin, Z. D., Thornalley, D. J. R., Barker, S., Marino, G., et al. (2016). Sequestration of carbon in the deep Atlantic during the last glaciation. *Nature Geoscience*, *9*(4), 319–324. https://doi.org/10.1038/ngeo2657

Yu, J., Menviel, L., Jin, Z. D., Thornalley, D. J. R., Foster, G. L., Rohling, E. J., et al. (2019). More efficient North Atlantic carbon pimp during the Last Glacial Maximum. *Nature Communications 10*, 2170. https://doi.org/10.1038/s41467-019-10028-z

Yu, Z., Colin, C., Ma, R., Meynadier, L., Wan, S., Wu, Q., et al. (2018). Antarctic Intermediate Water penetration into the northern Indian Ocean during the last deglaciation. *Earth and Planetary Science Letters*, *500*, 67–75. https://doi.org/10.1016/j.epsl.2018.08.006

Zahn, R., Winn, K., & Sarnthein, M. (1986). Benthic foraminiferal $\delta^{13}C$ and accumulation rates of organic carbon: *Uvigerina peregrina* group and *Cibicidoides wuellerstorfi*. *Paleoceanography*, *1*(1), 27–42. https://doi.org/10.1029/PA001i001p00027